COMPARISON OF MULTI-CAVITY ARRAYS FOR ON-CHIP WDM APPLICATIONS

A THESIS SUBMITTED TO
THE GRADUATE SCHOOL OF NATURAL AND APPLIED SCIENCES
OF
MIDDLE EAST TECHNICAL UNIVERSITY

BY

HAVVA ERDİNÇ

IN PARTIAL FULFILLMENT OF THE REQUIREMENTS
FOR
THE DEGREE OF MASTER OF SCIENCE
IN
ELECTRICAL AND ELECTRONICS ENGINEERING

JUNE 2019

Approval of the thesis:

COMPARISON OF MULTI-CAVITY ARRAYS FOR ON-CHIP WDM APPLICATIONS

submitted by HAVVA ERDİNÇ in partial fulfillment of the requirements for the degree of **Master of Science in Electrical and Electronics Engineering Department, Middle East Technical University** by,

Prof. Dr. Halil Kalıpçılar
Dean, Graduate School of **Natural and Applied Sciences** _____

Prof. Dr. İlkay Ulusoy
Head of Department, **Electrical and Electronics Eng.** _____

Assist. Prof. Dr. Serdar Kocaman
Supervisor, **Electrical and Electronics Eng., METU** _____

Examining Committee Members:

Prof. Dr. Gönül Turhan Sayan
Electrical and Electronics Engineering Dept., METU _____

Assist. Prof. Dr. Serdar Kocaman
Electrical and Electronics Eng., METU _____

Assist. Prof. Dr. Emre Yüce
Physics Dept., METU _____

Assist. Prof. Dr. Demet Asil Alptekin
Chemistry Dept., METU _____

Prof. Dr. Barış Akaoğlu
Physics Dept., Ankara University _____

Date: 12.06.2019

I hereby declare that all information in this document has been obtained and presented in accordance with academic rules and ethical conduct. I also declare that, as required by these rules and conduct, I have fully cited and referenced all material and results that are not original to this work.

Name, Surname: Havva Erdinç

Signature:

ABSTRACT

COMPARISON OF MULTI-CAVITY ARRAYS FOR ON-CHIP WDM APPLICATIONS

Erdinç, Havva
Master of Science, Electrical and Electronics Engineering
Supervisor: Assist. Prof. Dr. Serdar Kocaman

June 2019, 86 pages

Researches about the interaction of single atoms with electromagnetic field create the foundation of cavity quantum electrodynamics (CQED) technology. Microlasers, photon bandgap structures and quantum dot structures in cavities are the initial examples of Cavity Quantum Electrodynamics. This thesis is focused on the comparison of multi-cavity arrays for on-chip wavelength division multiplexing (WDM) applications in the weak coupling regime.

Firstly, single QD embedded cavity (cavity QD EIT) and cavity-cavity array (classical EIT) systems are compared in the weak coupling regime in terms of transmission, group delay, quality factor, and full width half maximum (FWHM) characteristics. Identical transmission characteristic is observed for both systems whereas group delay values of classical EIT is two times higher than the cavity-QD EIT surprisingly. Then, single QD embedded cavity-cavity array and triple cavity array systems are compared in the weak coupling regime. These structures are simulated with several different variables many times and results are compared with the calculations for both systems. Results show that it is possible to get different WDM characteristic with different configurations. Taking advantage of the unique capabilities of quantum technologies, on-chip WDM applications can create new opportunities for the latest developments in designing communication infrastructure.

Keywords: Cavity Quantum Electrodynamics, Quantum Dots, On-chip WDM

ÖZ

ÇOKLU KAVİTE DİZİLERİNİN ÇİP ÜSTÜ WDM UYGULAMALARI İÇİN KARŞILAŞTIRILMASI

Erdinç, Havva
Yüksek Lisans, Elektrik ve Elektronik Mühendisliği
Tez Danışmanı: Dr. Öğr. Üyesi Serdar Kocaman

Haziran 2019, 86 sayfa

Tekli atomların elektromanyetik alanla etkileşimi araştırmaları, Boşluk Kuantum Elektrodinamiği (CQED) teknolojisinin temelini oluşturur. Mikrolaserler, foton bant aralığı yapıları ve boşluklardaki kuantum nokta yapıları, Boşluk Kuantum Elektrodinamiğinin ilk örnekleridir. Bu tez, zayıf bağlanma rejiminde çip üzerinde dalga boyu bölmeli çoğullama (WDM) uygulamaları için çok boşluklu dizilerin karşılaştırılmasına odaklanmaktadır.

İlk olarak, kavite sistemine gömülmüş tek QD (kavite QD EIT) ve kavite-boşluk dizisi (klasik EIT) yapılarının, zayıf bağlanma rejiminde iletim, grup gecikmesi, kalite faktörü ve tam genişlikte yarım maksimum (FWHM) karakteristikleri açısından karşılaştırılmıştır. Her iki sistem için de benzer iletim karakteristiği gözlenirken, klasik EIT'nin grup gecikme değerleri, boşluk-QD EIT'den şaşırtıcı şekilde iki kat daha yüksektir. Daha sonra, boşluk kavite dizisi sisteminde gömülmüş tek QD ve üçlü boşluk dizisi zayıf bağlanma rejiminde karşılaştırılmıştır. Bu yapılar birçok farklı değişkenle pek çok kez simüle edilmiş ve sonuçlar her iki sistem için de hesaplamalarla karşılaştırılmıştır. Sonuçlar, farklı konfigürasyonlarla farklı WDM karakteristiklerin elde edilmesinin mümkün olduğunu göstermektedir. Kuantum teknolojilerinin benzersiz özelliklerinden yararlanarak, çip üzerinde WDM

uygulamaları, iletişim altyapısının tasarlanmasında en son gelişmeler için yeni fırsatlar yaratabilir.

Anahtar Kelimeler: Boşluk Kuantum Elektrodinamiği, Kuantum Noktalar, Çip Üzerinde WDM

To my family

ACKNOWLEDGEMENTS

Firstly, I would like to thank you my advisor Asst. Prof. Dr. Serdar KOCAMAN for his enlightening guidance and providing me the possibility to work in such a sophisticated facility.

I would like to thank Prof. Dr. Gönül TURHAN SAYAN, Asst. Prof. Dr. Emre YÜCE, Asst. Prof. Dr. Demet ASİL ALPTEKİN and Assoc. Prof. Dr. Barış AKAOĞLU for being on my thesis committee.

I would specially thank to Gülce TURHAN and Hasan İhsan TURHAN for opening the doors of your house. You always encouraged me to complete this job so I will always remember your support and friendship.

I would like to thank to Kübra ÇIRÇIR for her friendship and a lot of work for my place because I was far away.

Lastly, I am grateful to my mom, dad and sister for their endless love and support.

TABLE OF CONTENTS

LIST OF TABLES

TABLES

LIST OF FIGURES

FIGURES

CHAPTER 1

INTRODUCTION

Nanotechnology is a key research field to control and understand the behavior of the basic unit of matter that is to say atoms. The first appearance of the nanotechnology notion in our life made real by Richard Feynman in 1959 during his famous Caltech lecture that "There is plenty of room at the bottom: an innovation to enter a new field of physics." was the pioneer sentence of this lecture [1]. Richard Feynman believed that the formation of new structures by banding single atoms together was possible. His theory required the comprehensive understanding of fundamental laws of quantum physics to define a single atom behavior.

Another point is that the nanotechnology has actually been used for centuries with unawareness of this term. When we look at the ancient history, nanoparticles were used to create a sword with exceptionally sharp edges and craft glassware materials by Romans. On the other hand, the term of nanotechnology was used for the first time by Japanese scientific Norio Taniguchi in 1974 in his paper which describes a feature of an object with the nanometer scale [2]. Scientists have been studying about nanoparticles for decades but their research was ineffective because of not seeing the detailed structure of the nanoparticles. Then intervention of scanning tunneling microscope and atomic force microscope speeded up the nanotechnological research field since these devices allowed one to observe materials at an unprecedented atomic level [3]. With the help of detailed modeling and simulations of powerful computers production, atomic scaling visualization of nanoscale structures and characterization of material properties can be done easily [4]. These developments brought along the discovery of carbon nanotubes, semiconductor nanocrystals, and quantum dots [4]. Nanotechnology involves the synthesis, characterization, application, and design of materials on the nanometer

scale. At the nanometer scale, the behavior of individual molecules and interacting groups of molecules are more important than the macroscopic properties of the materials since scientists can affect the properties of materials in nanometer scale directly.

In normal life flow of the day, a single atom interacts with a single photon countless times which is the basic form of the interaction of matter and light. This entanglement is a promising activity for quantum communication and quantum computation. Atom-photon entanglement is the main research field of atomic physics and quantum optics for especially in the last century [5]. Lasers, photodiodes, detectors, light sources, light emitting diodes, and solar cells are invented out of the interaction between light and matter [5].

Light behavior is a controversial discussion since the seventeenth century [6]. Newton claimed that light rays consist of particles according to his mechanics' laws [7]. On the other hand, Huygens claimed that light rays consist of waves [7]. Scientists have been discussing what is light for centuries: particle or wave. In fact, light sometimes acts as a particle, sometimes as a wave [5].

Atom-photon entanglement initiated with the strongly coupled cavity quantum electrodynamics. There is an interaction between single atom with the photons in single-mode cavities [8]. In addition, it is possible that qubit entanglement between single atoms and an optical single photon. Cavity quantum electrodynamics (CQED) field has emerged as a result of these studies. In this thesis, we focus on cavity quantum electrodynamics and quantum dot device characteristics in large-scale optical communication applications. In addition, some of the studies in this thesis have been published as an article in Turkish Journal of Physics [9].

1.1. Quantum Dots

A quantum dot is about 2-10nm dimension nanoparticle and consists of 10-50 atoms [10]. Designing artificial atoms (quantum dots) and molecules (coupled quantum dots) is possible with the help of nano-fabrication technology with external voltages [11]. Electrically defined QDs, self-assembled QDs, and nanocrystals or colloidal QDs are the types of the quantum dot technology [12][13][14]. Electrically defined QD is realized by trapping an electron or a hole but there is no possibility for light interaction [12]. Self-assembled QDs and colloidal QDs have similarities in terms of optical characteristic. Self-assembled QDs have narrower homogenous broadening and higher electric dipole moment than colloidal QDs, therefore self-assembled QDs are more suitable than colloidal QDs for the applications of single emitter CQED [12]. In self-assembled QDs, cavity is constructed by removing holes from the structure and QD is embedded in the cavity. Also, this cavity is used to enclose light in-plane by distributed Bragg reflection and out-of-plane by total internal reflection as an optical cavity.

The growth of the self-assembled QD is not a well controllable activity that results in non-decisive spatial design [12]. This is why the size of the QD is uncontrollable. This results in differentiation in QD resonances and leads to a rather large inhomogeneous expansion of QD. It is generated by covering a low-band semiconductor with a surrounding material which has a higher bandgap [12]. This results in a three-dimensional coating for electrons and holes and the formation of discrete energy levels. With the ability to trap single atoms at discrete energy levels, semiconductor quantum dots provide predictive features for the quantum computation and single-photon sources. Application fields of quantum dots are memory chips, quantum computation, quantum cryptography, and quantum dot laser [14][15].

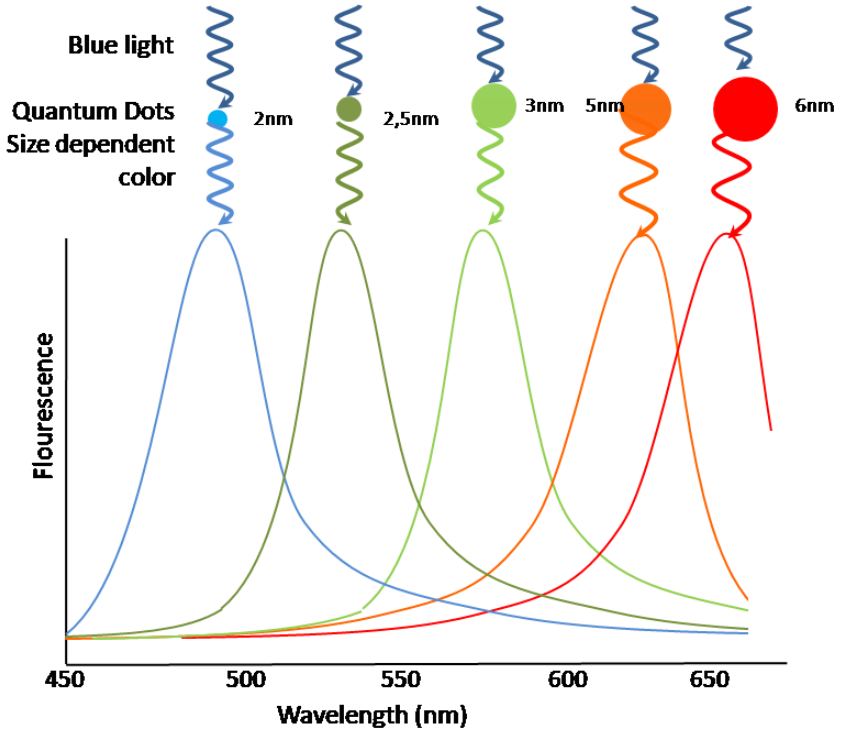

Figure 1.1. Size and Emission Wavelength of Quantum Dots (Figure has been prepared by using the corresponding figure in [16])

Different size of quantum dots have their maximum emission values at different wavelength values [14]. The emission wavelength of the QD for size-dependent color is shown in Figure 1.1 [17]. There is a size-tunable symmetrical fluorescent emission as function of QD size. When the size of the QD is increasing, it results in lower energy levels which consequently increases the emission wavelength.

A QD is characterized by discrete atomic-like states with energies that are determined by the QD radius R. These discrete QD states can be labeled as notations, such as 1S, 1P, and 1D which is shown in Figure 1.2 [14]. This represents the discrete absorption spectrum of a QD.

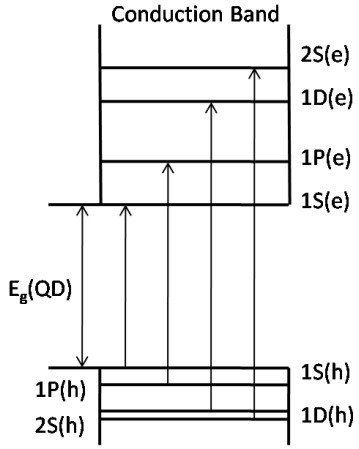

Figure 1.2. Quantum Dot Bandgap (Figure has been prepared by using the corresponding figure in [10])

Quantum dots are manipulated by Coulomb blockade and 3D confinement electrical effects. When the quantum dot devices are too small Coulomb blockade can be observed. The electrons inside the quantum dots generate strong Coulomb propulsion flowing of other electrons. So the devices will no longer follow Ohm's law [18]. Bandgap of quantum dot (Figure 1.2) is resizable by adding or removing electrons [19].

Scientists can calculate the bandgap of quantum-dot precisely in despite of the small size. When we assume that diameter of the QD is R, the difference between the lowest unoccupied energy level and highest occupied energy level is called bandgap of the QD [$E_g(QD)$]. The formula of the quantum dot bandgap is shown in Equation 1.1. This equation is called as Brus equation [20].

$$E_g(QD) \approx E_{g0} + \frac{\hbar^2\pi^2}{2m_{eh}R^2} \tag{1.1}$$

$$m_{eh} = \frac{m_e m_h}{m_e + m_h} \tag{1.2}$$

where $m_e$is the excited electron effective mass, m_h is the excited hole effective mass, $\hbar$ is Planck's constant and E_{g0} is bandgap energy of bulk semiconductor.

1.2. Optical Cavity

Optical cavities (resonators) allow the input light to circulate within the structure and then radiate the output light at a specific frequency or wavelength depending on the space parameters. Optical gain is obtained by using cavities. The control of the optical emission characteristics can be achieved by the materials placed inside these structures [20]. The conventional two-mirror resonator is referred to Fabry–Perot cavity which is shown in Figure 1.3.

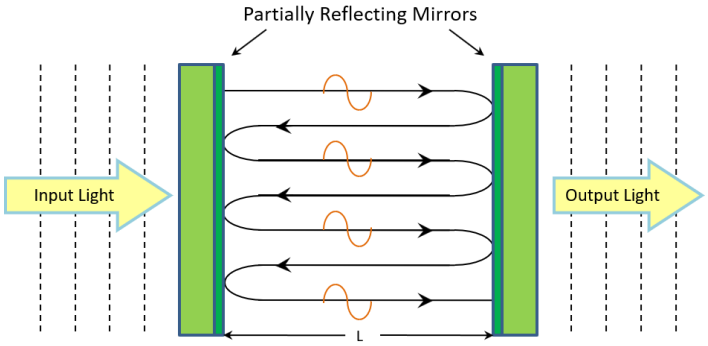

Figure 1.3. Fabry-Perot Optical Cavity (Figure has been prepared by using the corresponding figure in [13])

Optical cavity structure is shaped by two parameters: volume of the laser mode inside the active medium and stability of the optical cavity. In a stable resonator, the light beams on the axis remain in the resonator after multiple bounces, and very few off-axis axes are reflected in the orientation to bring them back into the center of the holes. The blue-colored regions correspond to stable cavities, the light regions are unstable in Figure 1.4. Six stable cases are marked in the diagram that all cases are on the borders of the stability regions. Geometric parameter of two-mirror optical cavities (M_1 and M_2) is defined as $g_1 = 1\text{-}L/R_1$ and $g_2 = 1\text{-}L/R_2$. R_1 and R_2 are the radii of the curvature of the mirrors and L is the distance between the mirrors. Then

we can sketch the stability diagram according to this inequality. Resonator stability condition is provided by $0 \leq g_1 g_2 \leq 1$ equation [21].

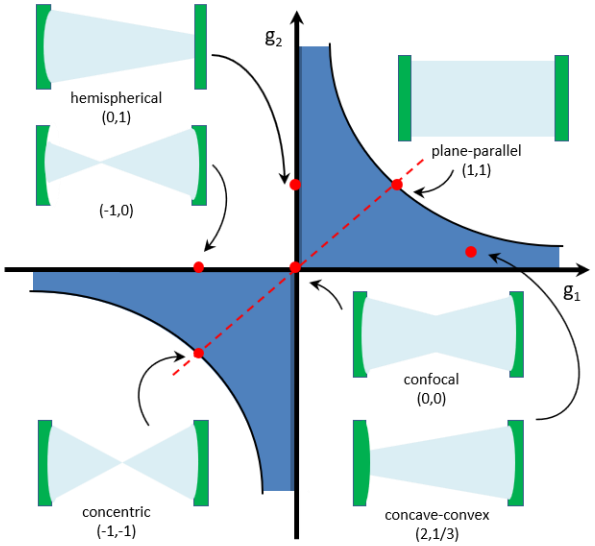

Figure 1.4. Stability Diagram of two-cavity (Figure has been prepared by using the corresponding figure in [16])

These types of resonators differ in their focal lengths of the mirrors and in their distances between the mirrors. Some beams have different shapes within the cavity and are thus chosen for different purposes. Five different types of stable two-mirror optical cavities are shown in Figure 1.5.

- plane-parallel $R_1 = R_2 = \infty$

- concentric (spherical) $R_1 + R_2 = L$

- confocal $R_1 + R_2 = 2L$

- hemispherical $R_1 = L$, $R_2 = \infty$

- concave-convex $R_1 >> L$, $R_2 = L - R_1$

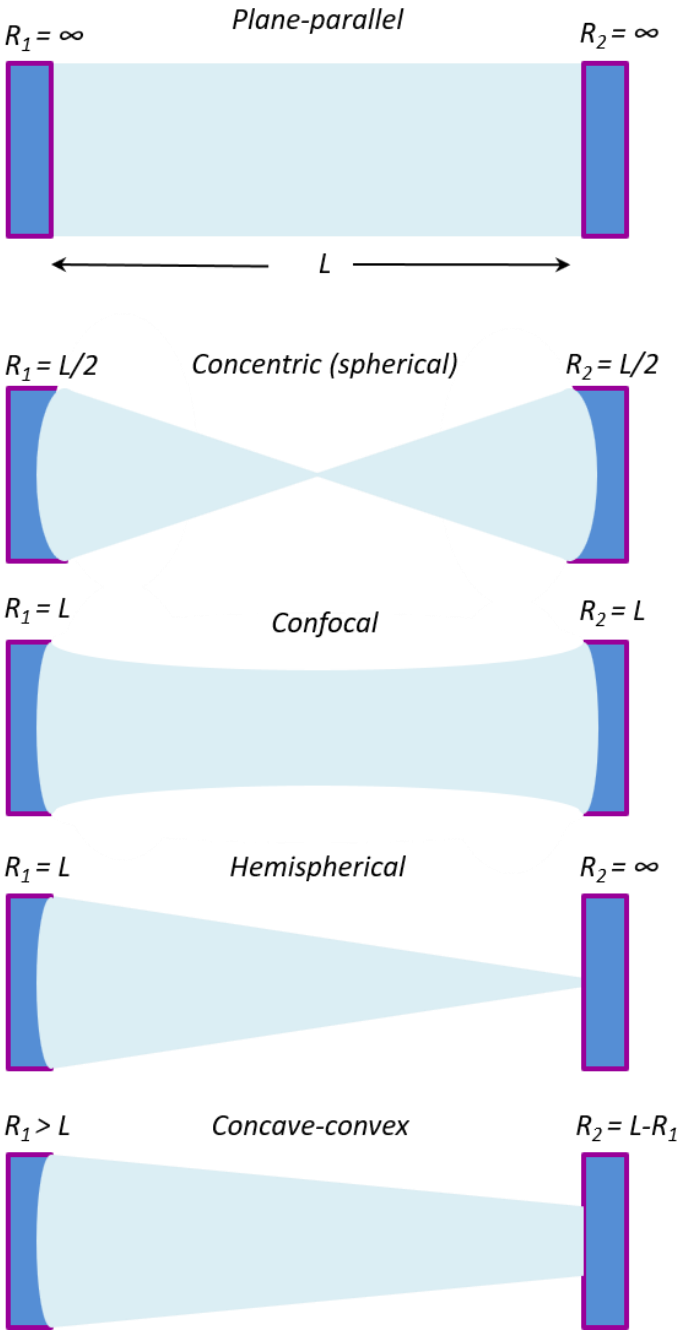

Figure 1.5. Types of two-mirror Optical Cavities (Figure has been prepared by using the corresponding figure in [16])

Optical microcavities are very useful for studying the basic physics of interaction between materials with the electromagnetic radiation, precise measurement science and quantum information processing [20]. Cavities are generally used in laser frequency stabilization applications. In addition, the spectral width of the lasers can be stabilized and it is possible to change the rate of spontaneous emission. When the frequency indecision of a laser in the visible region is reduced to 10^{-18}, the resulting laser strips are several MHz [20]. This makes a great contribution to the production of new generation precision measurements.

Transverse modes and frequency components of laser light are dependent to the optical cavity [22]. For this reason, sending light to an external optical space is a well-known laser light characterization method. At separate optical space, we can investigate the laser light as so we know the properties of the external space. In a sense, we use an optical space to characterize the other by sending laser light to an external resonator.

Cavity performance depends on factors including Q factor, loss of coupling and internal loss [20]. Laser light spectrum and resonator quality factor are decisive factors of optical cavity transmission function. The cavity transmission for a laser input with an extremely narrow optical spectrum is the maximum transmission of T_{max} (depends on reflection of the mirror), F (fineness), cavity subtlety and Δφrt, the round path optical phase [16].

$$T = \frac{T_{max}}{1 + \left(\frac{2F}{\pi}\right)^2 sin^2(\Delta\emptyset_{rt}/2)} \tag{1.3}$$

Fineness is defined as:

$$F = \frac{\pi\sqrt{r}}{1 - r} \tag{1.4}$$

At each round-trip factor (r) diminishes the wave amplitude. In consideration of the density reflection coefficients (R_1 and R_2), we have r = $\sqrt{R_1 R_2}$. Planar mirror plane length (L) of a plane wave in the cavity equals to L = Δφrt/2k where k= n2π / λ and n

is the refractive index of the material in the cavity. At Δφrt / 2 = qπ, the cavity transmission is maximum, where q is an integer or equivalent when 2kL = 2πq.

The resonance condition is then L / λ= q / 2 (where q = 1, 2, 3 ...). That is, half of the wavelength of the cavity length input light should be an integer. This means that the resonance monitoring of the optical cavity is a great way to detect small changes in the cavity length (in order of λ). The resonance condition at the wavelength or frequency of the input beam at a fixed cavity length:

$$\lambda_q = \frac{2L}{q} \tag{1.5}$$

$$\upsilon_q = \frac{cq}{2L} = q\upsilon_{FSR} \tag{1.6}$$

wherein the "free spectral range" is υ_{FSR}= c / 2L and the light speed in the cavity is c = c_0 / n. c_0 is the velocity of the light in a vacuum. The rotation of a photon from mirror 1 (M1) to mirror 2 (M2) and back to M1 (round-trip time) is only τrt = 1 / υ_{FSR}. The input laser and the laser FSR period are periodic to the laser of space. In contrast, the resonance condition in the cavity length should be an integer half-wavelength at a fixed laser frequency.

$$\mathrm{L}_q = q\frac{\lambda}{2} \tag{1.7}$$

Resonance width characterization is realized by finding the transmission peak full width half maximum values. Since we can vary the input cavity length to take off the cavity through the resonance and the laser, we obtain the following conditions on the resonance width:

$$\upsilon_{FWHM} = \frac{\upsilon_{FSR}}{F} \tag{1.8}$$

For large finesse (large survival probabilities), the photon lifetime is

$$\tau_p = \frac{1}{2\pi\upsilon_{FWHM}} \tag{1.9}$$

The resonator quality factor is 2π times the ratio of the total energy stored in the cavity divided by the energy lost in a single cycle. We can write the quality factor as

$$Q = 2\pi\upsilon_q\tau_p = \frac{\upsilon_q}{\upsilon_{FWHM}} = qF \tag{1.10}$$

1.3. Photonic Crystal Cavities

Photonic crystals (PhCs) are the class of optical media generated using the periodic modulation method of refractive index. PHCs are divided into three groups as one-dimensional (1D), two-dimensional (2D) and three-dimensional (3D) according to their geometrical structure [23]. Examples of these geometric constructs are shown in Figure 1.3.

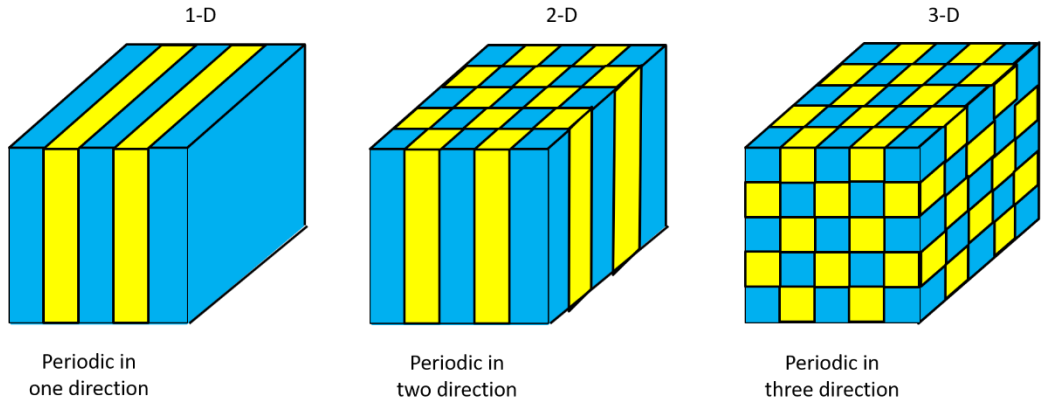

Figure 1.6. Examples of 1D (a), 2D (b), and 3D (c Photonic Crystals) (Figure has been prepared by using the corresponding figure in [16])

The geometric property of 1D PhCs permits periodic modulation only in one direction. Multi-layer film can be given as an example of 1D PhC structure that consists of alternating material layers with different dielectric constant [23]. It performs a mirror (a Bragg mirror) function for a specific frequency range and determines its location if there is a defect. 1D PhCs are used to improve the quality of the optical structure in structures such as lenses, dielectric mirrors and optical filters. 2D PHCs have a wider range of applications due to their optical transmittance in two directions. An example of 2D PHC is a bar system arranged periodically.

Another example of 2D PhC is a periodically arranged dielectric rod system.3D PHC has a permeability in all three directions so the number of applications that can be implemented is much more than 1D PhCs and 2D PhCs.

There are important similarities between solid state physics and PhC which are:

- Refractive index periodic modulation in a PhC creates a solid-state atomic lattice-like mesh

- The behavior of photons in a PhC provides due to lattice periodicity resemblance to electron and cavity behavior in an atomic lattice

Photonic bandgap is the most critical feature of determining the importance of a PhC. The photonic bandgap is used to express the energy or frequency range in which the light in the PhC is forbidden. If a complete periodic defect is observed, the defect has the same effect as a defect introduced to a semiconductor.

Building a defect around a single point is used to create an electromagnetic cavity, as we limit the waveguide to form a linear defect. As mentioned before, there is no way for light to escape because of the bandgap. The structure will limit the light only in the periodic plane, so there is a need for another method to prevent the light from escaping in the third direction.

Cavity is useful when it is desired to control the light evenly over a narrow frequency range or evenly over a long period of time. Besides, cavities are also used to release a particular photon corresponding to escape energy, or to influence the rate of atomic transitions associated with the absorption. Such transitions can suppress the atom by placing it in a photonic crystal where no suitable photon states exist, or it can be expanded by placing the atom in a cavity with a tightly concentrated photon state at exactly the transition frequency. This topic falls under the title of cavity quantum electrodynamics.

There is no point in catching the light finally if we do not confine the light in a cavity. For this reason, it is usually ensured that the cavity oscillations will have a

certain life time, meaning a way to escape the light will be provided. The easiest way to do this is placing a photonic crystal waveguide near the cavity.

The electric field $\vec{E}$ inside a resonator of volume a V is given by [11]:

$$\vec{E}(\vec{r}) = \sqrt{\frac{\hbar\omega}{2cV}}(\hat{a}(t) + \hat{a}^{\dagger}(t))u(\vec{r})\hat{u} \tag{1.11}$$

$\epsilon = \epsilon(\vec{r})$ is the dielectric function of the material

$u(\vec{r})$ is the single photon wave function normalized spatial part

$\hat{u}$ is the polarization of the field

ω is the photon frequency

$\hat{a}(t)$ is the annihilation operator

$\hat{a}^{\dagger}(t)$ is the creation operator

V is the cavity mode volume

Interaction Hamiltonian H_I of the dipole can be written in the form of optical transitions [11]:

$$H_I = -\vec{\mu}\cdot\vec{E} = \hbar g(\sigma^{+} + \sigma^{-})(\hat{a}(t) + \hat{a}^{\dagger}(t)) \tag{1.12}$$

The vacuum Rabi frequency inside the cavity

$$g = -\frac{\vec{\mu}\cdot\hat{u}}{\hbar}\sqrt{\frac{\hbar\omega}{2\epsilon V}u(\vec{r})} \tag{1.13}$$

$\sigma_{+} = |e\rangle\langle g| = \sigma_{-}^{\dagger}$ are the driven dipole lowering and raising operator that is taken to have an ground $|g\rangle$ and excited $|e\rangle$ states which determines the dipole-field coupling rate. Retaining only the energy conservation terms:

$$H_I = \hbar g(\sigma^{+}\hat{a}(t) + \hat{a}^{\dagger}(t)\sigma^{-}) \tag{1.14}$$

The mode volume V is defined as:

$$V = \frac{\int d^3\vec{r}\,\epsilon|E|^2}{\max\{\epsilon|E|^2\}} = \zeta\left(\frac{\lambda}{n}\right)^3 \tag{1.15}$$

There is a strong interaction between matter and light in applications of photonic crystal cavities [24]. In addition, the small mode volume and high Q factor are other basic features of the photonic crystal cavities. The main research fields of photonic crystal cavities are low threshold lasers, space quantum electrodynamics, high-fine filters, detection and sensing applications [25].

Spontaneous emission defines the stationary qubit to flying qubit conversion. In free space, one-electron atom decay or fall from level e to f by the emission of a photon and this situation is defined as spontaneous emission. In the beginning, enclosing domain of atom can modify the spontaneous emission rate and then there are different emitter properties that affect emission features [26]. Managing the spontaneous light emission is a crucial point for quantum optics because there are many application fields that emission affects the performance such as light-emitting diodes, miniature laser, solar energy harvesting. Indeed, manipulation of electromagnetic vacuum fluctuations should be supplied to control spontaneous emission [27]. Introduction of photonic crystals gives this advantage and has an impact to slow down or accelerate emitted light by adjusting vacuum of electromagnetic modes [28].

1.4. Cavity Quantum Electrodynamics

When the light is trapped in small mode volume using optical cavities, there is a strong electric field inside the cavity. This results in a very strong matter-light interaction. When the interaction strength is much lower than the system loss, the coupling between the cavity and the emitter field is called as weak coupling [12]. Conversely, strong interaction regime is achieved when the interaction strength is much higher than the system loss. Weak coupling results in low Q (quality factor.)

Cavity quantum electrodynamics (CQED) investigates the interaction between a single radiation field mode and a quantum emitter. The history of cavity quantum electrodynamics is based on nearly fifty years ago. Purcell is the pioneer of the

CQED [13]. The quantized matter with a quantized electromagnetic field defines the system.

There are possible applications of cavity-CQED:

1. Single-mode photon sources realization

2. All-optical (single photon) switches

3. Light standards based on quantum effects

4. Ultra-low threshold lasers

5. Coherent interfaces between matter and light (stationary and flying qubits)

In the beginning, CQED studies is realized by confining laser cooled atoms into Fabry-Perot cavities mostly. Experiments based on this system supply enviable controlling capability. Also, quantum computing and long-distance communication have been reported as an evidence of key displays of new technologies [12]. For this reason, atomic COED maintains to be an encouraging system for finding out basic physics and precise metrology. On the other hand, macroscopic dimension of Fabry-Perot and atom cooling and trapping needs of these systems make it difficult to scale these systems or develop integrated devices [12].

In quantum optics, the interaction of matter and light is the basic research topic. The interaction can be increased by trapping atoms in very thin cavities with small volume. The power of this interaction is determined by the atomic position of the light. As an advantage, higher intensity fields can be obtained with fewer photon numbers. This method is the basic approach of cavity quantum electrodynamics (CQED). In the first studies in CQED technology, the strong interaction excitation can be realized by passing atoms through the cavity.

Two-level approximated atom interaction with a single electromagnetic mode in the cavity is presented in Figure 1.7. Interaction results in quantum oscillation when the coupling strength (g) between an electromagnetic field and atom is higher than the

spontaneous emission rate (γ), the photon loss (κ) from the cavity, and the atom inverse transit time through the cavity [29].

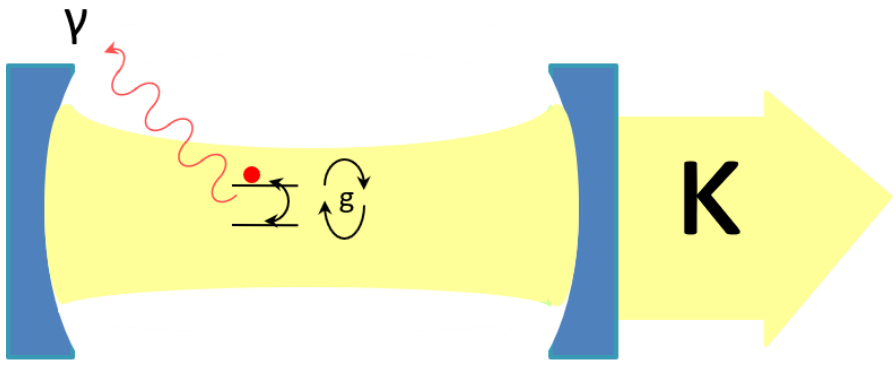

Figure 1.7. Cavity Quantum Electrodynamics (Figure has been prepared by using the corresponding figure in [16])

CQED research field is discrete photon modes coupling to atoms properties under high Q cavities. Quantum information processing and transmission quantum states, quantum mechanics of open systems, and measurement-induced decoherence are popular topics which can be realized with CQED systems.

All real physical systems are open systems which are partially coherent. Cavity quantum electrodynamics show quantum mechanics' coherence and decoherence [30]. The interaction between the quantized electromagnetic modes and the atoms inside the cavity is studied by the cavity quantum electromagnetic. Recent achievements in the nanofabrication studies of CQED systems have led to the application of these studies in the semiconductor field. In such systems, quantum wells and quantum dots are used as matter, and nanophotonic cavities are used to limit the light [31]. The mode volume of a nanophtonic cavity $\sim(\lambda/n)^3$ is much smaller than a volume that can be obtained with Fabry-Perot and the dipole moment

of QD (~ 30D) is much greater than an atom (~ 1D) [12]. In brief, achievement in semiconductor technology is promising in terms of scalability.

The growth of the QD is not a well controllable activity and this results in nonhomogeneous construction. This randomness presents challenges for the scalability of the QD-CQED platform, because it makes difficult to align the positioning and QDs spectrally to the spacing of the QDs, which prefers QDs as determinants. Although the large inhomogeneous expansion of QD represents a significant challenge for the scalability of the solid-state platform, there are several interesting ways to overcome a problem such as phonon coupling to circumvent the gap between QD and cavity.

Initial experiments in solid state CQED were focused on quantum well use in DBR cavities [12]. If there are fewer photons, the system does not show linearity even if there is strong interaction in the structure. Reaching a strong coupling regime with a single quantum emitter is more difficult than a quantum well as a result of a smaller total moment. To increase the coupling strength between the emitter and the optical field, cavities with very small mode volumes must be produced. A strong coupling between a single QD and an optical cavity can be provided with semiconductor nanocavities which leads to a new way to make optical CQED.

The coupling between the single quantum emitter and the optical cavity is studied in detailed by Jaynes Cummings Hamiltonian. Hamiltonian dynamics is described in Chapter 2. Cavity quantum electrodynamics yield is calculated with Q/V value. V is the mode volume of the cavity and Q is the quality factor of the factor of the cavity which is shown as $\omega_0/\Delta\omega$ (where ω_0 is the resonance frequency and $\Delta\omega$ is the cavity of the line width).

Photonic crystals have the highest yield among all nanophotonic cavities. The most important advantage of photonic crystals is that the mode volume is quite low. Considering efficiency equation of cavity quantum electrodynamics, increasing the Q value directly increases the efficiency, however, it decreases the processing speed

which is very important in information processing. Therefore, to improve cavity performance, reducing the mode volume would be better than increasing quality factor for computing applications.

1.5. Cavity Quantum Electrodynamics

Quantum technology gives opportunities for accomplishing fast computation, reliable communication, and high accuracy metrology. Cavity arrays, quantum dots, and spin chains are the physical systems which are utilized for performing quantum networks. Moreover, they play a role in realizing quantum technology devices.

Quantum technology offers to manage classical computations with quantum computing, successful cryptosystem, the higher data rate of classical communication through quantum channels and solving capability of complicated problems easily [32]. Information technology and quantum physics alliance brought a new start of quantum information technology devices such as quantum cryptosystems and quantum computers [33]. Quantum cryptography devices are promising for reliable communication and quantum computers supply.

During the data transmission from the transmitter to the receiver, the signal is attenuated and there is a loss of information over the fiber optic cable. The loss of photons results in data transmission errors over the entire communication. In classical communication, an amplifier solves the problem but quantum states of photons cause disturbance according to no-cloning theorem [34]. Quantum repeaters are developed to surpass the photon loss by reducing the required distance that a single photon needed to be travel [35].

Optical fibers can be used as quantum channels entanglement between photons up to 50 km fiber. Quantum cryptography provides a quantum key distribution of up to 100 km, but these developments have a distance limitation for quantum communication.

Quantum systems manipulation, storage, and communication of data are the main interest field of quantum information technology. Superposition and entanglement properties make the system better than classical communication. In large-scale quantum communication, fixed quantum bits (qubits) are the building blocks of the stable and addressable quantum memories. It is possible to move and entangle quantum information between memories for even macroscopic distance.

Designing quantum memories with the atomic systems have superior results since qubits can be accumulated during a long time by the internal electronic states. When transferring the quantum information among qubits, photons are crucial carrying elements with low perturbation capability.

Quantum communication is provided by entangling the quantum memories (atom) with the communication channel (photon). The main aim of the quantum information technology is building a reliable bridge for quantum data transmission between a quantum channel and quantum memory. For this reason long distance quantum communication, quantum teleportation of matter and quantum internet are allowed to be realized [36]. Store, process, and communication flows of quantum information technology is realized according to the quantum physics law.

In quantum information technology, data is transported from input state to output state with a quantum state with an external electromagnetic field for a while. Quantum information processing technology takes advantage of coupled-cavity arrays.

Quantum physics and quantum mechanics developments take advantage of information technology because they are the basic tools for quantum information process. Electrons and photons are basic building blocks for encoding information of transportation and processing information through a single photon. Confidential messages can be transmitted firmly by quantum communication [37].

1.6. Wavelength Division Multiplexing

In long-distance communication (>1000km), a high amount of data signals is sent between cities, lands and through the mountains. This amount of data transmission with classical communication is expensive and hard. To find a solution to this problem, fiber optic cables have been started to use at the first time 1970's [34]. Fiber optic technology has replaced the classical information system and figures a pioneer in telecommunication infrastructure. Speed, distortion, signal losses, capacity and power limitation are basic disadvantages of communication networks but fiber optic suppresses many of them [38].

Fiber optic cable is consisting of core, cladding and plastic coating. The core is central material and the light flow area of the transmission. Fiber optic cable is as thin as about 10 μm diameter. It has a high bandwidth capability so it is suitable for high load large scale communication.

Wavelength division multiplexing (WDM) is a way of receiving or sending multiple data streams in a single optical fiber at the same time. Speed, latency or bandwidth values do not change during the operation because the transmission operation is made simultaneously. WDM can consist of multiple wavelengths at the same time. Also, addition and subtraction data channels give flexibility to WDM system which is comprised of the multiplexer for combining optical signals and demultiplexer for separating optical signals. Transmission of fiber optic line between WDM transmitter and receiver is shown in Figure 1.8.

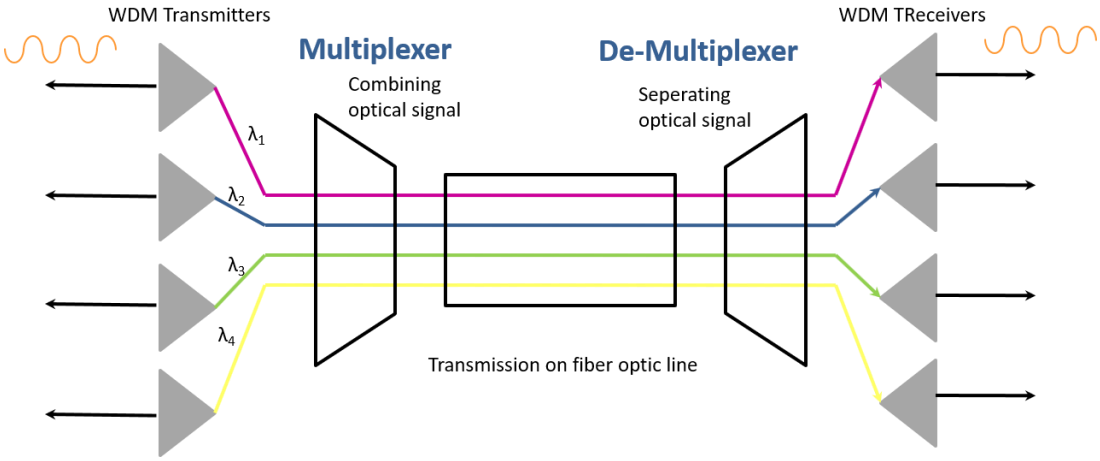

Figure 1.8. WDM Multiplexer and Demultiplexer Scheme (Figure has been prepared by using the corresponding figure in [16])

There are two types of WDM: DWDM (dense wavelength division multiplexing) and CWDM (coarse wavelength division multiplexing) as shown in Figure 1.6. CVDM provides 4, 8 or 18 channel variation for the fiber variation capacity [39]. The space between the channels is 20 nm over the full range of 1260 to 1670 nm [40]. The capacity of the channel number is low but the cost of the application is cheaper than the DWDM. DWDM has a capacity of up to 32 channels for passive and up to 160 channels for active applications of DWDM [41]. Especially for long distance communication like submarine cables and the high number of channels DWDM are more suitable than CWDM.

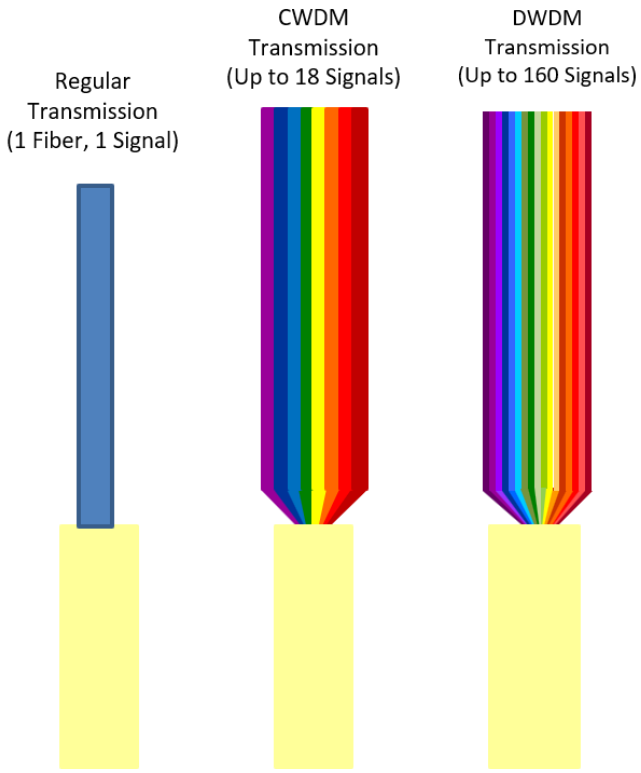

Figure 1.9. WDM Types (Figure has been prepared by using the corresponding figure in [16])

Especially large scale communication, increasing the network capacity without laying additional fiber cable is an advantage for telecommunication companies [38]. DWDM increases the capacity of submarine cables and broaden the lifetime of fiber optic cables being used. This situation decreases the cost of the infrastructure work.

1.7. Outline of the Thesis

Generally, the thesis aims to compare and analyze a single embedded QD cavity-cavity array and triple cavity array systems in terms of transmission spectrum and the generated temporal group delays characteristic. Simulation results of the systems are discussed and give suggestions for optimum performance in the on-chip WDM system application. Chapter 2 gives detailed theoretical model about the cavity quantum dot and multi-cavity subsystem dynamics. The interactions between the

quantum dots and cavities are examined by using these techniques. Then in chapter 3 both systems are compared and the equations of the theoretical models are solved. We applied the same spectrum characteristic for appropriate comparison. Also, the simulation results are figured and discussed in this chapter. Finally, in chapter 4 the results and on-chip WDM application of this system are given and discussed.

CHAPTER 2

THEORY OF QUANTUM DOT-CAVITY QED SYSTEMS

Quantum mechanics is a branch of physics that studies the behavior of atom and light in atomic and subatomic level. Electrodynamics studies the classical theory of electric and magnetic phenomena. Quantum electrodynamics is the combination of quantum mechanics and electrodynamics. In this chapter, the fundamental working theory of coupled QD-cavity system is studied.

2.1. Theory of Operation

In small cavities, atoms and photons behaviors are totally different than in free space. Comprehensive understanding of the interaction between the cavity and excited atoms requires both classical and quantum physics. Quantum physics studies about atomic and subatomic levels of matter and energy behavior nature. It is the science of the very small world. With developing technology atoms and ions can be placed the desired location inside the cavity to realize strong atom-cavity interaction.

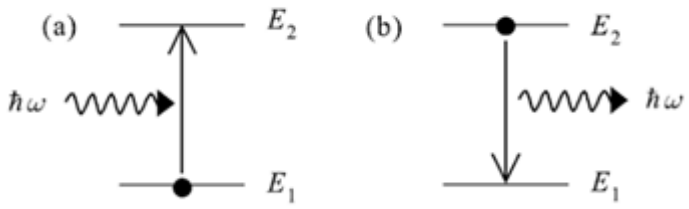

Figure 2.1. Absorption (a) and Spontaneous Emission (b) Optical Transition Between Quantized Energy Levels

When the two measured energy levels (E_2-E_1) surrounding an atom jump between E_1 and E_2, the angular frequency of light (ω) is absorbed or emitted. While the absorption process is seen as the photon destruction from the light beam by simultaneous stimulation of the atom (Figure 2.1 (a)). The emission process corresponds to the addition of a photon to the light field and simultaneous excitation of the photon. We imagine that the atom is initially low and at the time t = 0, the angular frequency of light beam is on. At a later time, the atom evokes the jump, and a photon is absorbed from the light beam. Similarly, in the emission process shown in Figure 2.1 (b), the atom is removed at time t = 0. Typically, a photon of the angular frequency is ignored after a period equals to the radiation life of the excited state. After these processes are completed, it is said that the atom passes a level 1→ 2 and vice versa. Stimulated emission processes are not considered in these figures.

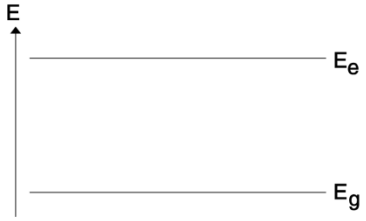

Figure 2.2. Two-Level Atom

Atom and light interaction is generally improved in terms of the two-level atomic approach in quantum operation. This approach can be applied when the frequency of the light runs across atom optical transition. The condition is specified in equation (E_2-E_1=ħω) and schematically shown in Figure 2.2. There are many quantum levels of atoms and there will be many possible optical transitions between them. However, it is paid regard to only the specific transition in the two-level atom approach that provides equivalents and ignores all other levels. It is customary to label the upper (E_e) and lower (E_g) levels 1 and 2, respectively.

When evaluated physically, the two-level approach mainly deals with resonance properties. The light beam induces dipole emissions at the atom and then re-emits at the same frequency in classical light-atom interaction. When the light frequency is equal to the atom natural frequency, the interaction between the atom and light will be strong. In addition, the power of dipole oscillations will be large. On the other hand, when the frequency of light is not close to the atom natural frequency, then the applied oscillations will be small and the atom-light interaction will be small. In other words, atom-light interaction is quite strong in the resonance state. Therefore, it is a good approach to ignore situations in which there is no resonance.

It is clear that the assumption that only resonance levels are important is an approach. In most cases, the approximation is very good. By the way, the presence of non-resonance levels may be indirectly significant. When the atom is at level 2, it can also switch to lower levels. This causes atomic loss from the system of thought and effectively reduces the atom-light interaction. Thus, the simplest way to incorporate other levels into analysis is to include damping terms.

2.2. Hamiltonian Dynamics

Generally, in a molecular, atomic and solid-state environment there are a number of energy eigenstates. The spectral lines are associated with permissible transitions between the two of these energy eigenstates. According to many physical thoughts, it is sufficient to take into account only two of these possible energy values. Laser transition can be shown as example, phenomenological relaxation processes between the upper laser level to lower laser level is produced by laser pumping. This simple model indicates a two-level atom that is mathematically equivalent to a spin 1/2 particle in an external magnetic field since the spin can only be parallel or parallel to this field. It has two areas: energy levels and eigenvalues of energy.

Hamiltonian Dynamics clarifies a two-level atom interaction with a single electromagnetic field mode. The total Hamiltonian equation is [42]:

$$\mathcal{H} = \mathcal{H}_{\text{field}} + \mathcal{H}_{\text{atom}} + \mathcal{H}_{\text{int}} \quad (2.1)$$

The total Hamiltonian equation consists of three pieces: field ($\mathcal{H}_{\text{field}}$), atom ($\mathcal{H}_{\text{atom}}$), and interaction ($\mathcal{H}_{\text{int}}$).

$$\mathcal{H}_{\text{field}} = \hbar\omega_C \hat{a}^+\hat{a} \quad (2.2)$$

$$\mathcal{H}_{\text{atom}} = \hbar\omega_A \hat{\sigma}_{eg}\hat{\sigma}_{ge} \quad (2.3)$$

$$\mathcal{H}_{\text{int}} = -\hat{d}.\hat{E} = g\hbar(\hat{a}\hat{\sigma}_{eg} + \hat{a}^+\hat{\sigma}_{ge}) \quad (2.4)$$

$$\mathcal{H} = \hbar\omega_C \hat{a}^+\hat{a} + \hbar\omega_A \hat{\sigma}_{eg}\hat{\sigma}_{ge} + g\hbar(\hat{a}\hat{\sigma}_{eg} + \hat{a}^+\hat{\sigma}_{ge}) \quad (2.5)$$

Longitudinal quasi-mode in the cavity where ω_C is the resonant frequency of the cavity and ω_A is the frequency spacing between the atoms' ground and excited states.

Non-interacting two level atom:

Spin-flip operator: $\hat{\sigma}_{ge} = |g\rangle\langle e|$

$$\hat{E} = \varepsilon \sin(kx)\,(\hat{a} + \hat{a}^+) \quad (2.6)$$

$$\varepsilon = \sqrt{\frac{\hbar\omega_c}{2\epsilon_0 V}} \quad (2.7)$$

The interaction energy in the dipole approximation:

$$\mathcal{H}_{\text{int}} = -\hat{d}.\hat{E} = -\wp\varepsilon \sin(kx)\,(\hat{\sigma}_{eg} + \hat{\sigma}_{ge})(\hat{a} + \hat{a}^+) \quad (2.8)$$

Rotating wave approximation:

$$\mathcal{H}_{\text{int}} = g\hbar(\hat{a}\hat{\sigma}_{eg} + \hat{a}^+\hat{\sigma}_{ge}) \quad (2.9)$$

Single photon frequency:

$$g = -\frac{\wp\varepsilon}{\hbar}\sin(kx) \quad (2.10)$$

$$\wp = \langle e|e\hat{\vec{r}}|g\rangle \quad (2.11)$$

â is the annihilation operator [43]

2.3. Quantum Dot and Coherent Light Interaction

In this section, the model system created by a single emitter will be considered. Under ideal conditions, cavity losses and emitter relaxation are negligible, which is known to produce a Rabi oscillation of the coupled system. In this case, spontaneous

emission is becoming a reversible process. In other words, the cavity can be reabsorbed and diffused again when the emitted photon is emitted by the emitter. The angular frequency of the Rabi oscillation is proportional to the force of the atom-field combination [13]. Consequently, the vacuum field at the emitter's site is directly related to the volume of impact of the omega cavity. At a specific location, vacuum field fluctuations concentration ability is allowed to measure thanks to this event.

Practically, microcavity has not an excellent structure. Mirrors limited reflection due to the absorption and conduction allows the photon leakage through the cavity. An open cavity leads to another way for the radial relaxation of the spontaneous emission at the emitter to the continuity of non-resonant modes. This kind of decoherence is slow enough on the scale of the period of Rabi oscillation that affects the emitter throughout the process. The unified system has an extinguished Rabi oscillation.

Rapid decoherence processes cause excessive damping where the transmitter is regularly loosened to the ground state. However, while the cavity damping results in decoherence process, it is possible to adapt the quality factor value of the emitter to the spontaneous emission value of the emitter, and in particular the spontaneous emission speed, by adjusting the force of both the transmitter-field coupling and the cavity loss.

Cavity quantum electrodynamics (CQED) studies and controls the simplest light-matter interaction. Firstly, in relation to quantum optics, an emitter is an atom or a collection thereof, while the electromagnetic field is limited to a high fineness [44]. There are many applications of CQED such as sources of decoherence and are radiative and dissipation non-radiative decays, internal loss processes in the emitter, propagation and plasmons leakage losses the in the resonator.

The vacuum Rabi frequency of the quantum dot which is also called as coupling strength (g) must be higher than the dipole decay rate of quantum dot and cavity for

a full switch between quantum dot and cavity that depends on position and dipole alignment [45]. When a quantum dot (transition frequency ω_d) resonates to the PC cavity on the ω_c frequency, the dot emission is changed depend on the g, γ and field decay rate $\kappa = \omega_c / (2Q)$ parameters [46]. Coupled cavity-QD system eigenfrequency equation is acquired by solving Interaction Hamiltonian [46]:

$$\omega_{\pm} = \frac{\omega_c + \omega_d}{2} - i\frac{(\kappa + \gamma)}{2} \pm \sqrt{\left(\frac{\kappa - \gamma + i(\omega_c - \omega_d)}{2}\right)^2 - g^2} \qquad (2.12)$$

Up to the square root is real or imaginary, the equation has two limits, one real and the other imaginary. If the square root is imaginary, quantum dot interaction is called as strong coupling regime. In this case, there is an oscillation at two frequencies with single decay rate. If both of the eigenvalues are real, it results in cavity and quantum dot decay rates. This phenomenon is called as weak coupling regime.

2.3.1. Strong Coupling

A single mode of cavity is suitable for transition in the initial state. The atomic and vacuum field pair generate in a quantity of quantum energy shifting back and forth between this vacuumed atom and mode at the frequency [47]. Cavity and atomic mode interaction force is linear in the field, and therefore smaller cavity volumes intensify the vacuum area of the mode and generate wider frequencies. The basic dynamics of the atom-field system is reversible so as the system is isolated. Similarly, the atomic transition binds to continuous radiation modes and thus encounters spontaneous deterioration of the population as well as reduced polarization. Strongly connected systems are systems in which the Rabi dynamics can exist even though there is a short period of time despite the fact that dispersion. In strong interaction, atomic field coupling force g (half of the Rabi frequency) is faster than any basic distributor speed. Also, there are high-Q cavities. Photon transitions between atoms and radiation field can be observed periodically. This

situation results in entanglement of atoms and photons and contributes to the base of many quantum information processing procedures.

The eigenvalues of the coupled cavity-QD can be found from Equation 2.12 regarding $g \geq \frac{\kappa}{2}$ under strong coupling regime [48]. When square root must be

$$\omega_{\pm} = \frac{\omega_c + \omega_d}{2} - i\frac{(\kappa + \gamma)}{2} \pm \sqrt{g^2 - \left(\frac{\kappa - \gamma + i(\omega_c - \omega_d)}{2}\right)^2} \qquad (2.13)$$

In strong coupling regime, cavity-QED allows modifying light emitters optical properties in a unique way such as modifying the dynamics from incoherent to coherent and non-linear interaction at low intensities. Atom number detection, nonlinear optics and conditional phase shifts on single photons operations require strong coupling interaction between the cavity and dipole emitter [45].

2.3.2. Weak Coupling

In the weak coupling regime, both eigenenergies have the same true fraction so that Rabi oscillation disappears [13]. Spontaneous emission is a nonreversible process and the emitter experiences a monotonic relaxation towards the baseline when it is in empty space. However, it is possible to control the spontaneous emission adaptation and the spontaneous emission rate of the emitter. Under weak coupling regime, cavities are in low-quality factor-Q and it results in level shifts and spontaneous transition adjustment [46].

Weak coupling situation occurs when dissipation suppresses coherent coupling in QD-cavity systems [47][49]. For this reason, decay rate is the dominant factor. In this systems, eigenfrequency equations can be found with Equation 2.12 regarding $\kappa \gg (\omega_c - \omega_d, g) \gg \gamma$.

Under weak coupling, eigenfrequencies are represented as:

$$\omega_+ = \omega_d + i\frac{g^2}{\kappa} \quad (2.14)$$

$$\omega_- \approx \omega_c + i\kappa \quad (2.15)$$

In weak coupling regime, optical properties of light emitters can be modified by cavity-QED in a unique way such as manipulating spatial emission pattern and natural lifetime.

2.4. Purcell Factor

A two-level system is spontaneously weakened by interacting with vacuum continuity at a rate proportional to the spectral density of the modes per volume at the transition frequency [50]. When the intensity of the modes in the space is changed, large oscillations may occur in the amplitude. The maximum intensity of modes in terms of cavity modes occurs at quasi-mode resonance frequencies and can substantially surpass the corresponding free space density. Normalizing an increased mode density of the space per unit volume to the free space mode density gives the spontaneous emission to increase Purcell factor. The refractive index (n) should be added to this statement to account for emissions within the dielectric.

An atom falling along the transition mode width will show an improvement in the rate of spontaneous deterioration by the Purcell factor. Proper cavity design and self-distortion can be prevented to work at these resonance frequencies. The rigorous developments of Purcell's physical model are presented on the basis of calculating the continuity mode density. In order to cover the Purcell effect, the corresponding atomic transition characteristics must be considered in the design of the micro-cavities. It is important to use a small volume because improvements with Q manipulation alone are limited by the spectral width of the transition.

Transition rate of an excited emitter when there is an interaction with the continuum of vacuum modes is [51]:

$$\frac{dP_e(t)}{dt} = \left(\frac{2\pi}{\square^2}\right) |\langle \mu_{12} E \rangle|^2 D_{free}(\omega) \quad (2.16)$$

μ_{12} is dipole moment and there is free space density of states:

$$D_{free} = \frac{\omega^2 V}{\pi^2 c^3} \tag{2.17}$$

In free space, spontaneous emission can be represented as:

$$\Gamma_{free} = \frac{\omega_0^3 \mu_{12}^2}{3\pi\varepsilon_0 \square c^3} \tag{2.18}$$

When the emitter is encircled by a cavity, the vacuum density of states is changed.

D_{free} is changed with D_{cav}:

$$D_{cav}(\omega) = \frac{\kappa}{2\pi V} \frac{1}{(\kappa/2)^2 + (\omega_{cav} - \omega)^2} \tag{2.19}$$

Spontaneous emission results in:

$$\Gamma_{cav} = \frac{3Q\lambda^3}{4\pi^2 V} \frac{\kappa^2}{4(\omega - \omega_{cav})^2 + \kappa^2} \frac{\left|\mu_{12}\hat{E}\right|^2}{|\mu_{12}|^2} \Gamma_{free} \tag{2.20}$$

Quality factor (Q) of cavity is:

$$Q = \omega_{cav}/\kappa \tag{2.21}$$

When there is a perfect matching between dipole orientation and in resonance, spontaneous emission enhancement is shown as:

$$\Gamma_{cav} = \frac{3}{4\pi^2} \left(\frac{\lambda_0^3}{V}\right) Q \Gamma_{free} \tag{2.22}$$

When there is a perfect matching between dipole orientation and off resonance, spontaneous emission enhancement is shown as:

$$\Gamma_{cav} = \frac{3}{16\pi^2} \left(\frac{\lambda_0^3}{V}\right) Q^{-1} \Gamma_{free} \tag{2.23}$$

The result is showed that excited emitter natural lifetime is not a constant. It can be modified using high-Q cavities. Inside a cavity or resonator, spontaneous emission rate enhancement is called as Purcell factor.

$$\mathrm{P} = \frac{3}{4\pi^2} \left(\frac{\lambda}{\mathrm{n}}\right)^3 \frac{\mathrm{Q}}{\mathrm{V}} \tag{2.24}$$

Purcell factor formula is consisting of quality factor (Q) and refractive index (n) within a cavity volume (V). Higher Q-factor, smaller mode volume and smaller

spectral width of the emitter than the cavity width results in large Purcell factor values. High Q-factor and small mode volume of the cavities must be required to detect the cavity QED effects. While designing microcavities Purcell factor must be considered.

2.5. Rabi Splitting

Vacuum Rabi splitting describes the high anticrossing between cavity-mode dispersion relations and atom-like emitter. When the coupling strength surpasses the system dissipation and the energy, there is an energy change between atom and cavity photon. Quantum coherent oscillation from coupled systems to quantum superposition at different quantum states pave the way for quantum information processing thanks to Rabi splitting. Also, emission, scattering, absorption, transmission and reflection properties are comprehensively investigated in quantum and semi-classical systems. Plasmon quantization deepens the concept of Rabi splitting into plasmon-plasmon coupling systems and plasmon-cavity.

Jaynes-Cummings-Hamiltonian equation is used to determine the single emitter interaction in a single cavity.

$$H_{jC} = \frac{1}{2}\hbar\omega_0\sigma_z + \hbar\omega_a{}^{+}a + \hbar g(a\sigma^{+} + a^{+}\sigma^{-}) \tag{2.25}$$

The equation comprises of coupling constant (g), Pauli spin operator (σ_z), cavity resonance frequency (ω_a), transition frequency (ω_0), and atomic state lowering operator (σ^-). The excited state (|e>), ground state (|g>) and photon number state (|n>) of the two-level system is regarded by Hamiltonian to couple states |n,e> with |n+1,g> . Therefore, H is defined as:

$$H_n = \hbar\left(n + \frac{1}{2}\right)\omega\begin{pmatrix}1 & 0\\ 0 & 1\end{pmatrix} + \hbar\begin{pmatrix}-\delta/2 & g\sqrt{n+1}\\ g\sqrt{n+1} & \delta/2\end{pmatrix} \tag{2.26}$$

The detuning is shown as:

$$\delta = \omega_0 - \omega \tag{2.27}$$

There are eigenenergies in resonance:

$$E_{2n} = \hbar\left(n + \frac{1}{2}\right)\omega - \hbar g\sqrt{n+1} \tag{2.28}$$

$$E_{1n} = \hbar\left(n + \frac{1}{2}\right)\omega + \hbar g\sqrt{n+1} \tag{2.29}$$

The eigenstates (dressed states) are represented in resonance:

$$|2n\rangle = (|e,n\rangle - |g,n+1\rangle)/\sqrt{2} \tag{2.30}$$

$$|1n\rangle = (|e,n\rangle + |g,n+1\rangle)/\sqrt{2} \tag{2.31}$$

$c_{en}(t)$ and $c_{gn+1}(t)$ coefficients are motion coupled equations which are shown as:

$$\dot{c}_{en} = -i\frac{\delta}{2}c_{en} - ig\sqrt{n+1}c_{gn+1} \tag{2.32}$$

$$\dot{c}_{gn+1} = i\frac{\delta}{2}c_{gn+1} - ig\sqrt{n+1}c_{en} \tag{2.33}$$

This gives a state initially in the upper state:

$$|c_{en}(t)|^2 = \cos^2(g\sqrt{n+1}t) \tag{2.34}$$

$$\left|c_{gn+1}(t)\right|^2 = \sin^2(g\sqrt{n+1}t) \tag{2.35}$$

Even if n = 0 (no photon or interaction with the vacuum) there is:

$$|c_{e0}(t)|^2 = \cos^2(gt) \tag{2.36}$$

g is called vacuum Rabi-frequency.

Rabi oscillation is defined as quantum energy transfer between the emitter and field mode in striking difference to the irreversible exponential decay into free space of an excited atom. Periodic energy transfer has an analogy with two coupled pendula. Under the high Q factor regime, the coupling constant g is called as Rabi frequency.

2.6. Coherent Interaction in Cavity Array

Photonic cavity arrays are used for producing wide-range photonic integrated circuits [52]. To calculate the interaction equation of cavity array systems, $\hat{c}$ represents the basonic annihilation operator of the cavity and κ_1 is the external cavity decay rate. Input and output relations are given as:

$$\hat{a}_{out} = \hat{b}_{in} - \sqrt{\kappa_1}\hat{c} \quad (2.37)$$

$$\hat{b}_{out} = \hat{a}_{in} - \sqrt{\kappa_1}\hat{c} \quad (2.38)$$

The motion equations are:

$$\frac{d\hat{c}}{dt} = -i[\hat{c}, H] - \Gamma\hat{c} + \sqrt{\kappa_1}(\hat{a}_{in} + \hat{b}_{in}) \quad (2.39)$$

$$\frac{d\hat{\sigma}_-}{dt} = -i[\hat{\sigma}_-, H] - \gamma\hat{\sigma}_- + \sqrt{\dot{\gamma}}\dot{\hat{\sigma}}' \quad (2.40)$$

$$H = \omega_c\hat{c}^\dagger\hat{c} + \omega_r\hat{\sigma}_-\hat{\sigma}_+ + [g\hat{\sigma}_+\hat{c} + h.c] \quad (2.41)$$

In this formula $\hat{\sigma}_-|e\rangle = |g\rangle$ and $\hat{\sigma}_+|g\rangle = |e\rangle$, so $\hat{\sigma}_- = |g\rangle\langle e|$ and $\hat{\sigma}_+ = |e\rangle\langle g|$. This means that $\hat{\sigma}_- = \hat{\sigma}_+$.

When we rewrite the Hamiltonian equation:

$$H = \omega_c\hat{c}^\dagger\hat{c} + \omega_r\hat{\sigma}_-\hat{\sigma}_+ + [g\hat{\sigma}_+\hat{c} + g^*\hat{c}^\dagger\hat{\sigma}_-] \quad (2.42)$$

If Hamiltonian equation is transformed into commutation relations:

$$[\hat{c}, H] = \omega_c[\hat{c}, \hat{c}^\dagger\hat{c}] + \omega_r[\hat{c}, \hat{\sigma}_-\hat{\sigma}_+] + g[\hat{c}, \hat{\sigma}_+\hat{c}] + g^*[\hat{c}, \hat{c}^\dagger\hat{\sigma}_-] \quad (2.43)$$

$$[\hat{\sigma}_-, H] = \omega_c[\hat{\sigma}_-, \hat{c}^\dagger\hat{c}] + \omega_r[\hat{\sigma}_-, \hat{\sigma}_-\hat{\sigma}_+] + g[\hat{\sigma}_-, \hat{\sigma}_+\hat{c}] + g^*[\hat{\sigma}_-, \hat{c}^\dagger\hat{\sigma}_-] \quad (2.44)$$

Under single mode standard normalization, annihilation operator and ascending (descending) operators are:

$$[\hat{c}, \hat{\sigma}_+] = [\hat{c}, \hat{\sigma}_-] = 0 \quad (2.45)$$

$$[\hat{c}, \hat{c}^\dagger] = 1 \quad (2.46)$$

The total cavity decay rate is represented as 2Γ and relevant to intrinsic cavity decay (κ_0). Their relation is showed as $\Gamma = (\kappa_0 + 2\kappa_1)/2$. $\hat{\sigma}_-$ and $\hat{\sigma}_+$ are descending and ascending operators of two-level QD interaction with transition frequency ω_r . The vacuum noise operator ($\dot{\hat{\sigma}}'$) and total decay rate ($\dot{\gamma}$) are between quantum dot and cavity. H is the Hamiltonian operator which consists of g coupling strength between the cavity mode and the dipolar transition from excited ($|e\rangle$) to ground ($|g\rangle$) states of the QD. ω_c and ω_r represent the resonant frequency of cavity mode and transition frequency proportionally. The Hamiltonian equation is given as:

Commutation relations can be simplified as:

$$[\hat{c}, H] = \omega_c \hat{c} + g^* \hat{\sigma}_- \tag{2.47}$$

$$[\hat{\sigma}_-, H] = \omega_r [\hat{\sigma}_-, \hat{\sigma}_+] \hat{\sigma}_- + g[\hat{\sigma}_-, \hat{\sigma}_+] \hat{c} \tag{2.48}$$

If there is a weak excitation limit:

$$[\hat{\sigma}_-, \hat{\sigma}_+] = 1 - 2\hat{\sigma}_+ \hat{\sigma}_- \tag{2.49}$$

$$[\hat{\sigma}_-, H] = \omega_r \hat{\sigma}_- + g\hat{c} \tag{2.20}$$

Motion equations are simplified when the noise term is ignored:

$$\frac{d\hat{\sigma}_-}{dt} = -i\omega_r \hat{\sigma}_- - ig\hat{c} - \gamma \hat{\sigma}_- \tag{2.51}$$

$$\frac{d\hat{c}}{dt} = -i(\omega_c \hat{c} + g^* \hat{\sigma}_-) - \Gamma \hat{c} + \sqrt{\kappa_1}(\hat{a}_{in} + \hat{b}_{in}) \tag{2.52}$$

2.7. Multi Cavity-QD Transport Matrix Rabi Splitting

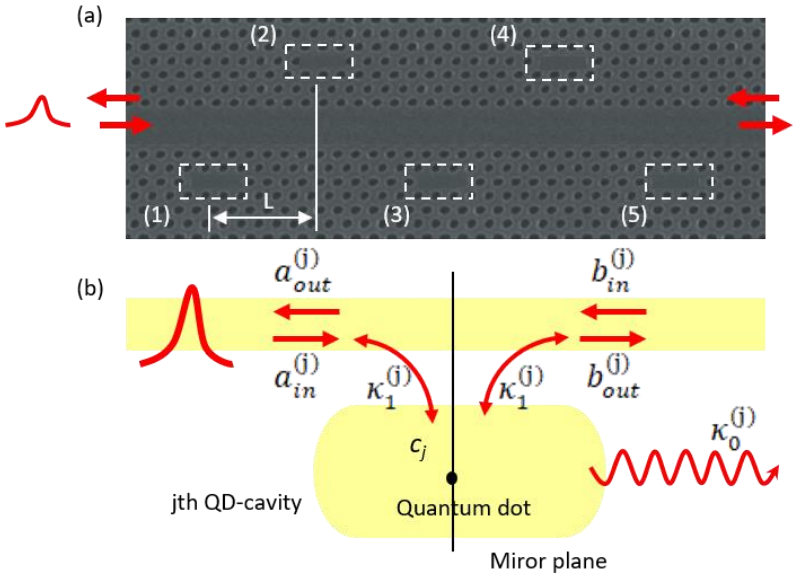

Figure 2.3. (a) N Side Coupled Cavities at a Distance L Periodic Waveguide-Resonator Structure. (b) The jth QD-Cavity Subsystem (Figure has been prepared by using the corresponding figure in [47])

An isolated QD subsystem and single cavity interaction are derived from the Heisenberg equations of motion derived as 2.32 and 2.33.

$$\frac{d\hat{\sigma}_{-,j}}{dt} = -i[\hat{\sigma}_{-,j}, H_j] - \gamma_j \hat{\sigma}_{-,j} - \sqrt{\gamma_j'}\sigma_j', \tag{2.53}$$

$$\frac{d\hat{c}_j}{dt} = -i[\hat{c}_{-,j}, H_j] - \Gamma_j c_{-,j} + i\sqrt{\kappa_{1,j}}(\hat{a}_{in}^{(j)} + \hat{b}_{in}^{(j)}) \tag{2.54}$$

In the weak coupling regime, we can omit the Langevin noises [53]. When the motion equations are solved, here is the matrix form consist of transport relation in frequency domain

$$\begin{pmatrix} \hat{b}_{in}^{(j)}(\omega) \\ \hat{b}_{out}^{(j)}(\omega) \end{pmatrix} = T_j \begin{pmatrix} \hat{a}_{in}^{(j)}(\omega) \\ \hat{a}_{out}^{(j)}(\omega) \end{pmatrix} \tag{2.55}$$

The transport matrix is written as:

$$T_j = \frac{1}{a_j + \kappa_{1,j} - \Gamma_j} \begin{pmatrix} -\kappa_{1,j} & \alpha_j - \Gamma_j \\ \alpha_j - \Gamma_j + 2\kappa_{1,j} & \kappa_{1,j} \end{pmatrix} \tag{2.56}$$

where $a_j = i(\omega - \omega_{c,j}) + |g_j(\vec{r})|^2 / [i(\omega - \omega_{r,j}) - \gamma_j]$

$(\omega - \omega_{c,j})$ and $(\omega - \omega_{r,j})$ presents the detuning between cavity mode and the input field. $\delta_j \equiv \omega_{c,j} - \omega_{r,j}$ represents cavity-QD detuning. N-coupled cavity-QD transportation equation system can be derived by cascading transport matrix. The generalized transportation equation is shown as:

$$\begin{pmatrix} \hat{b}_{in}^{(N)}(\omega) \\ \hat{b}_{out}^{(N)}(\omega) \end{pmatrix} = T_N T_0 \dots T_0 T_2 T_0 T_1 \begin{pmatrix} \hat{a}_{in}^{(1)}(\omega) \\ \hat{a}_{out}^{(1)}(\omega) \end{pmatrix} \tag{2.57}$$

T_0 represents the transport matrix from the waveguide with a phase propagation θ. Multicavity array transportation equations can be written with Figure 2.2.

2.8. Cavity-QD Transport Matrix

After the Fourier transform applied, equations turn into:

$$-i\omega\hat{\sigma}_-(\omega) = -i\omega_r\hat{\sigma}_-(\omega) - ig\hat{c}(\omega) - \gamma\hat{\sigma}_-(\omega) \tag{2.58}$$

$$-i\omega\hat{c}(\omega) = -i\omega_c\hat{c}(\omega) - ig\hat{\sigma}_-(\omega) - \Gamma\hat{c}(\omega) + \sqrt{\kappa_1}(\hat{a}_{in}(\omega) + \hat{b}_{in}(\omega)) \tag{2.59}$$

If the motion equations are solved regarding weak excitation limits [50], the transport relation in the frequency domain becomes as follows:

If $\hat{c}(\omega)$ is solved:

$$\hat{c}(\omega) = \frac{\sqrt{\kappa_1}\left(\hat{a}_{in}(\omega) + \hat{b}_{in}(\omega)\right)}{-i(\omega - \omega_c) + \Gamma - \frac{|g|^2}{i(\omega - \omega_{r1}) - \gamma}} \tag{2.60}$$

The input-output relations are:

$$\hat{a}_{out}(\omega) = \hat{b}_{in}(\omega) - \frac{\kappa_1\left(\hat{a}_{in}(\omega) + \hat{b}_{in}(\omega)\right)}{-i(\omega - \omega_c) + \Gamma - \frac{|g|^2}{i(\omega - \omega_{r1}) - \gamma}} \tag{2.61}$$

$$\hat{b}_{out}(\omega) = \hat{a}_{in}(\omega) - \frac{\kappa_1\left(\hat{a}_{in}(\omega) + \hat{b}_{in}(\omega)\right)}{-i(\omega - \omega_c) + \Gamma - \frac{|g|^2}{i(\omega - \omega_{r1}) - \gamma}} \tag{2.62}$$

Relations are simplified into:

$$\hat{b}_{in}(\omega) = \left(\frac{\kappa_1}{-\alpha + \Gamma - \kappa_1}\right)\hat{a}_{in}(\omega) + \left(\frac{-\alpha + \Gamma}{-\alpha + \Gamma - \kappa_1}\right)\hat{a}_{out}(\omega) \tag{2.63}$$

$$\hat{b}_{out}(\omega) = \left(\frac{\alpha - \Gamma + 2\kappa_1}{\alpha - \Gamma + \kappa_1}\right)\hat{a}_{in}(\omega) + \left(\frac{\kappa_1}{\alpha - \Gamma + \kappa_1}\right)\hat{a}_{out}(\omega) \tag{2.64}$$

where $\alpha = i(\omega - \omega_c) + \frac{|g|^2}{i(\omega - \omega_r) - \gamma}$

If the motion equations are solved regarding weak excitation limits, the transport relations in the frequency domain becomes as follows:

$$\begin{pmatrix} \hat{b}_{in}(\omega) \\ \hat{b}_{out}(\omega) \end{pmatrix} = \frac{1}{\alpha - \Gamma + \kappa_1}\begin{pmatrix} -\kappa_1 & \alpha - \Gamma \\ \alpha - \Gamma + 2\kappa_1 & -\kappa_1 \end{pmatrix}\begin{pmatrix} \hat{a}_{in}(\omega) \\ \hat{a}_{out}(\omega) \end{pmatrix} \tag{2.65}$$

where $\alpha = i(\omega - \omega_c) + \frac{|g|^2}{i(\omega-\omega_r)-\gamma}$

This matrix form represents a single QD embedded in a cavity. In chapter 3, cavity-cavity array, single embedded QD cavity-cavity array and triple cavity array matrix equations are formulated with the same form.

CHAPTER 3

IMPLEMENTATION AND CHARACTERIZATION OF MULTICAVITY QUANTUM ARRAYS

Electromagnetically induced transparency (EIT) was suggested by Harris et al in 1990 [54]. Quantum systems optical properties can be manipulated by quantum interference effects [54]. EIT removes the effect of a medium on an electromagnetic radiation propagating beam [55]. The basic philosophy of removing the effect of a medium can be supplied by stopping of electrons when moving under applied field at specific frequencies. An immobile electron does not make a contribution to the dielectric constant [56]. Electromagnetically induced transparency (EIT) provides use of many technologies like quantum information, lasing without inversion, optical delay, nonlinearity enhancement, precise spectroscopy, pushing frontiers in quantum mechanics and photonics [57]

Also, slow light definition arose from EIT by decreasing the speed of light in an atomic gas. In an ultracold atomic gas, light speed is reduced to 17 m/s [58]. This development brings to mind the question that if it can be possible to stop the light. Storing light in an optical medium can be possible when the light is stopped. Quantum memories have been built with single atoms recently [59]. Encoding quantum bits with this method is a realizable technique by taking advantage of the light stop feature. Quantum communication and quantum computing technology can be developed by the discovery of EIT technology.

Applications of EIT can be listed as:

1. Quantum memory

2. Optical switches

3. Quantum information processing

4. Lasing without inversion

5. Reduction of the speed of light

6. All-optical wavelength converters for telecommunication

7. EIT commercial and fundamental applications in quantum optics and atomic physics include

High-quality optical semiconductor cavity production techniques provide an opportunity to analyze cavity-quantum electrodynamics effects in solid-state materials. Quantum dots inside a photonic crystal, micropillar, and microdisk resonators are up-and-coming systems in cavity-quantum electrodynamics in solid-state materials.

There are two interaction types between cavity and QD: strong and weak excitation regimes which are varying according to coupling strength (g) value [42][49]. If the cavity decay rate (2Γ) is much higher than the coupling strength, the interaction between the quantum dots and cavities is weak coupling ($|g(r)| < \kappa, \gamma$) [12]. In the opposite case, strong coupling excitation ($|g(r)| > \kappa, \gamma$) regime is valid [12]. Strong coupling has many application fields such as conditional phase shifts on single photons, atom number detection and nonlinear optics [45]. In strong coupling, high transmission to high reflection transform of the cavity is realized with a dipole that results in conditional phase shifts on single atoms. On the other hand, a dipole can convert the cavity between high transmission to high reflection in weak excitation regimes too.

3.1. Cavity-QD EIT and Classical EIT

At first, one cavity interacting with a quantum dot subsystem is examined. In chapter 2.5, the motion equations are solved regarding weak excitation limits. Single QD

embedded cavity (cavity-QD EIT) and cavity-cavity array (classical EIT) subsystems are represented in Figure 3.1.

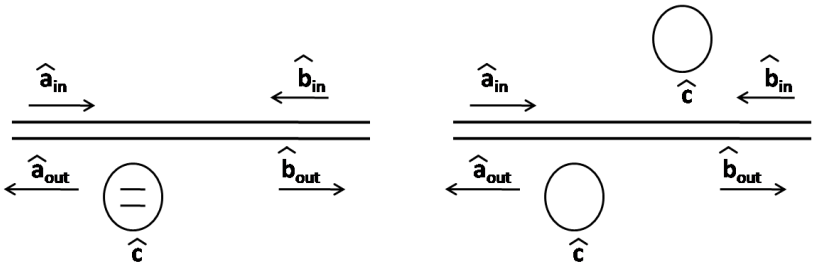

Figure 3.1. Cavity-QD (a) and Classical EIT (b)

The transport matrix relation of cavity-QD EIT in the frequency domain becomes as follows:

$$\begin{pmatrix} \hat{b}_{in}(\omega) \\ \hat{b}_{out}(\omega) \end{pmatrix} = \frac{1}{\alpha - \Gamma + \kappa_1} \begin{pmatrix} -\kappa_1 & \alpha - \Gamma \\ \alpha - \Gamma + 2\kappa_1 & -\kappa_1 \end{pmatrix} \begin{pmatrix} \hat{a}_{in}(\omega) \\ \hat{a}_{out}(\omega) \end{pmatrix} \tag{3.1}$$

where $\alpha = i(\omega - \omega_c) + \frac{|g|^2}{i(\omega - \omega_r) - \gamma}$

Transportation equation of classical EIT is obtained regarding the coupling strength value equals to zero because there is any QD in this system. Thus, waveguide transport relation needs to be added in phase form as $\theta=2\pi$. When we regard this explanation, the transport matrix follows:

$$\begin{pmatrix} \hat{b}_{in}(\omega) \\ \hat{b}_{out}(\omega) \end{pmatrix} = \frac{1}{\beta_1 - \Gamma + \kappa_1} \begin{pmatrix} -\kappa_1 & \beta_1 - \Gamma \\ \beta_1 - \Gamma + 2\kappa_1 & -\kappa_1 \end{pmatrix} \begin{pmatrix} 0 & e^{j2\pi} \\ e^{j2\pi} & 0 \end{pmatrix} \frac{1}{\beta_2 - \Gamma + \kappa_2} \begin{pmatrix} -\kappa_2 & \beta_2 - \Gamma \\ \beta_2 - \Gamma + 2\kappa_2 & -\kappa_2 \end{pmatrix} \begin{pmatrix} \hat{a}_{in}(\omega) \\ \hat{a}_{out}(\omega) \end{pmatrix} \tag{3.2}$$

where $\beta_j = i(\omega - \omega_{cj})$

The spectral character of the cavity-QD subsystem should be analyzed to understand the physical behavior of the systems. The transmission and reflection values can be

calculated by $t = \hat{a}_{out}/\hat{b}_{in}$ and $r = \hat{a}_{out}/\hat{a}_{in}$, respectively. In addition, the transmitted field phase is defined as $\phi = \angle(\hat{b}_{out}/\hat{a}_{in})$.

Extrinsic cavity decay rate (κ_1) value is taken as 50 times of the intrinsic cavity decay rate (κ_0) in Figure 3.2. To make the equations into a simpler form, extrinsic cavity decay rates are accepted as equal to each other in all single cavity calculations thereafter in this thesis ($\kappa_2=\kappa_1=\kappa$).

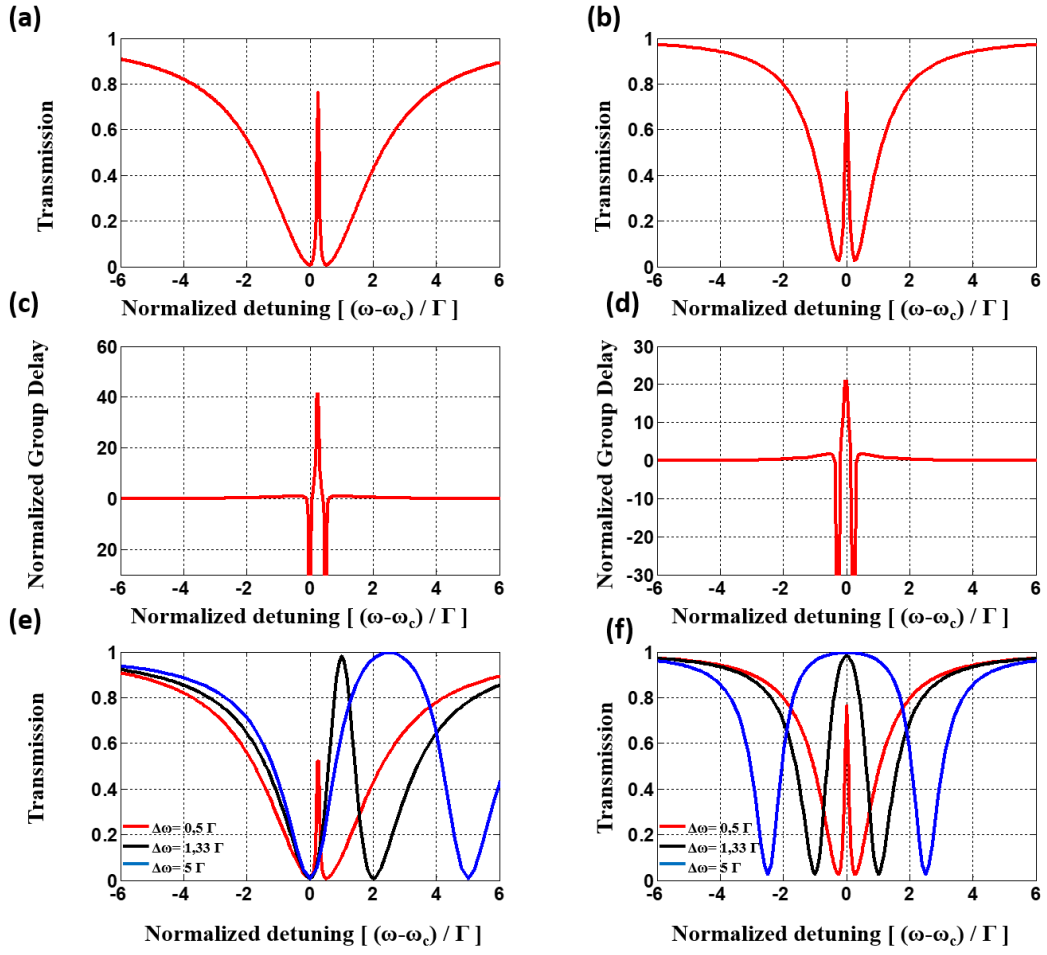

Figure 3.2. The transmission spectrum for classical EIT (Cavity-QD EIT), a(b). The generated group delay and calculated phase (insets) corresponding to Classical EIT (Cavity-QD EIT), c(d). The transmission spectrum in a(b) is differentiated for various detuning, e(f).

In Figure 3.2, single QD embedded cavity (cavity-QD EIT) and cavity-cavity array (classical EIT) systems are compared in terms of transmission spectra, the phase of the transmitted fields and group delay ($d\phi/d\omega$) values. The transmission characteristics [Figure 3.2 (a) and Figure 3.2 (b)] and the corresponding phase/group delay values [Figure 3.2 (c) and Figure 3.2 (d)] look similar for both the cavity-QD EIT and classical EIT cases.

Figure 3.2 (a) shows the spectral transmission characteristic of the classical EIT case. The coupling strength value is assumed to be zero because the coherent interaction occurs if and only if the bus waveguide phase accumulations is an integer multiple of 2π. The group delay corresponding to calculated transmission spectra is given in Figure 3.2 (c). The resonant frequencies ($-\Delta\omega/2$, $\Delta\omega/2$) are modified by varying first cavity (ω_{c1}) and second cavity (ω_{c2}) resonant frequencies. $\Delta\omega$ values are changed as 0.5Γ, 1.33Γ and 5Γ which are shown for the red, black and blue lines, respectively [Figure 3.2 (f)].

Figure 3.2 (b) shows the spectral transmission characteristic of the cavity-QD EIT case. The group delay corresponding to calculated transmission spectra is given in Figure 3.2 (d).

Transmission and phase group delay equations of classical EIT and cavity QD EIT should be analyzed in detail to comment and understand the simulation results in Figure3.2. First of all, Equation 3.1 is solved for cavity-QD EIT transmission in phase form:

$$t(\omega) = \frac{\omega^2 - g^2 - \frac{\gamma\kappa_0}{2} + i\omega\left(\gamma + \frac{\kappa_0}{2}\right)}{\omega^2 - g^2 - \frac{\gamma\kappa_0}{2} - \gamma\kappa_1 + i\omega\left(\gamma + \frac{\kappa_0}{2} + \kappa_1\right)} \tag{3.3}$$

In the transmission spectrum, transmission peaks at $\omega=0$ so we should look at transmission values at this point.

$$t(\omega = 0) = \frac{g^2 + \frac{\gamma\kappa_0}{2}}{g^2 + \frac{\gamma\kappa_0}{2} + \gamma\kappa_1} \tag{3.4}$$

Derivation of transmission (Equation 3.3) at transparency peak value (ω=0) gives the phase delay. The equation is normalized with total cavity decay rate (1/2Γ):

$$\frac{\tau_c}{\tau_{life}}(\omega = 0) = \frac{\kappa(g^2 - \gamma^2)(2\kappa + \kappa_0)}{\left(g^2 + \frac{\kappa\kappa_0}{2} + \kappa\gamma\right)\left(g^2 + \frac{\kappa\kappa_0}{2}\right)} \tag{3.5}$$

Then, the same calculations are repeated for triple cavity system. Then, the transmission equation is derived from Equation 3.2 at $t(\omega = 0)$. The normalized detuning between the cavities is Δω so first and second resonant cavities are -Δω/2 and Δω/2, respectively.

$$t(\omega = 0) = \frac{\left(\frac{{\kappa_0}^2}{4} + \frac{\Delta\omega^2}{4}\right)}{\left(\kappa\kappa_{0+}\frac{{\kappa_0}^2}{4} + \frac{\Delta\omega^2}{4}\right)} \tag{3.6}$$

$$\frac{\tau_c}{\tau_{life}}(\omega = 0) = \frac{\kappa\left(\frac{\Delta\omega^2}{4} - \frac{{\kappa_0}^2}{2}\right)(2\kappa + \kappa_0)}{\left(\frac{\Delta\omega^2}{4} - \frac{{\kappa_0}^2}{4}\right)\left(\frac{\Delta\omega^2}{4} - \frac{{\kappa_0}^2}{4} + \kappa\kappa_0\right)} \tag{3.7}$$

Extrinsic cavity decay rate is quietly higher than intrinsic cavity decay rate ($\kappa \gg \kappa_0$). Total decay rate (γ) is assumed that equal to κ_0 [53]. The transmission equations of cavity-QD EIT and classical EIT in a simpler form of peak values is shown as:

$$t(\omega = 0) \approx \frac{g^2}{g^2 + \kappa\kappa_0} \tag{3.8}$$

$$t(\omega = 0) \approx \frac{\Delta\omega^2/4}{\kappa\kappa_0 + \Delta\omega^2/4} \tag{3.9}$$

When we compare the Equation 3.8 and Equation 3.9, Classical EIT and Cavity QD EIT transmission coefficient values converge to each other at g=Δω/2

$$-\frac{\tau_c}{\tau_{life}}(\omega = 0) \approx \frac{\kappa(2\kappa + \kappa_0)}{(g^2 + \kappa\kappa_0)} \tag{3.10}$$

$$\frac{\tau_c}{\tau_{life}}(\omega = 0) \approx \frac{2\kappa(2\kappa + \kappa_0)}{\left(\Delta\omega^2/4 + \kappa\kappa_0\right)} \tag{3.11}$$

Phase delay equations of classical EIT and cavity-QD EIT in Equation 3.15 and Equation 3.16 show that classical EIT is two times higher than the cavity-QD EIT

system. This interesting result gives a chance to the designer for better results in wavelength division multiplexing (WDM).

After that, transmission and group delay values are calculated for both systems with various coupling strength and normalized detuning values. In Figure 3.3 (a) and Figure 3.3 (b) extrinsic cavity decay rate, κ, is adjusted from $10\kappa_0$ to $250\kappa_0$. Normalized detuning between the resonant cavities, $\Delta\omega$, is adjusted to 0.5Γ and coupling strength, g, is adjusted to 0.25Γ. Simulation results show that extrinsic cavity decay rate variation affects transmission and generated group delay values directly. As expected, transmission values are identical for cavity-QD EIT and classical EIT cases. In addition, group delay values of classical EIT system are two times higher than the cavity-QD EIT system as it is shown in Equation 3.15 and Equation 3.16.

Then, the coupling strength value is adjusted from 0.1Γ to 0.75Γ for cavity-QD EIT case and the normalized detuning between the resonant cavities are adjusted from 0.2Γ to 1.5Γ in classical EIT case. At the same time, extrinsic cavity decay rate value is taken as $50\kappa_0$.

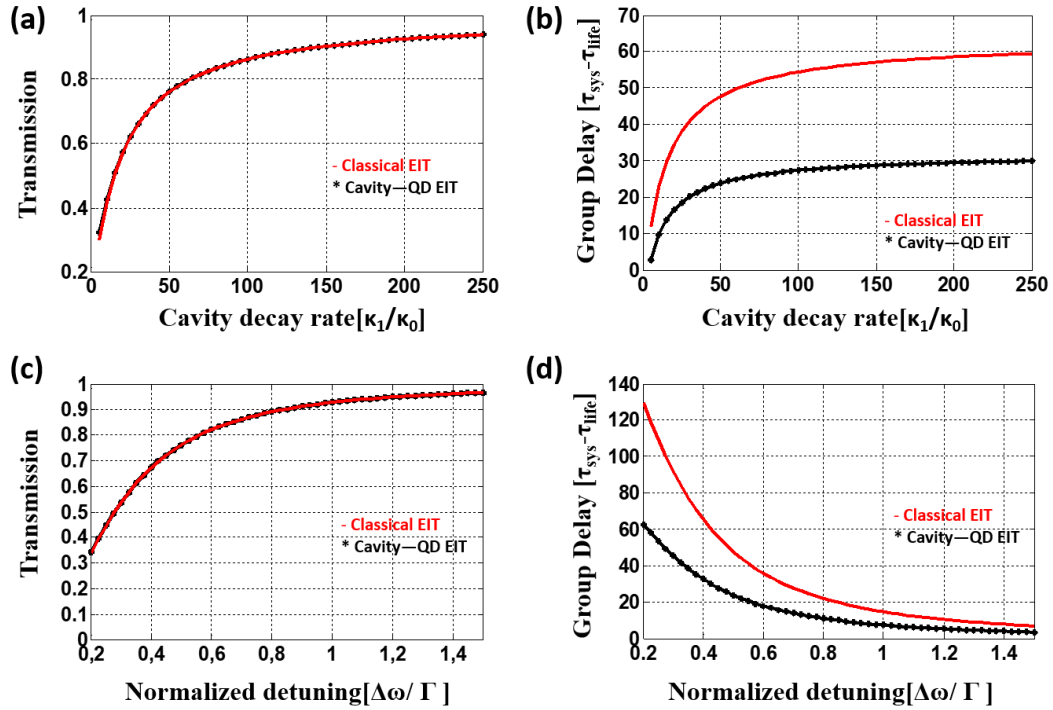

Figure 3.3. Comparison of transmission spectrum (a) and generated group delay (b) of single embedded QD in cavity array and cavity-cavity array with the coupling strength of 0.5Γ. Same transmission (c) and group delay (d) graphs are repeated for $\kappa=50\ \kappa_0$

Afterward, the simulations showed in Figure 3.3 (a) and Figure 3.3 (b) are recalculated with smaller coupling strength (0.1Γ) and normalized detuning (0.2Γ) values. Calculations of the transmission and group delay values are figured in Figure 3.4 (a) and Figure 3.4 (b). The calculations show that smaller coupling strength and normalized detuning result in smaller transmission values. On the other hand, group delay values are higher than the previous results. Also, the transmission values of both systems are identical to each other and group delay of classical EIT is two times higher than the cavity-QD EIT.

In Figure 3.4 (c) and Figure 3.4 (d), the extrinsic cavity is equaled to $\kappa=10\kappa0$ and the calculations are repeated with Figure 3.4 (a) and Figure 3.4 (b) intervals. Lower extrinsic cavity decay rate values result in smaller transmission value and group delay. When we analyzed the results the transmission and group delay rates of the

systems are destroyed when smaller extrinsic cavity decay rate is smaller than as we expected.

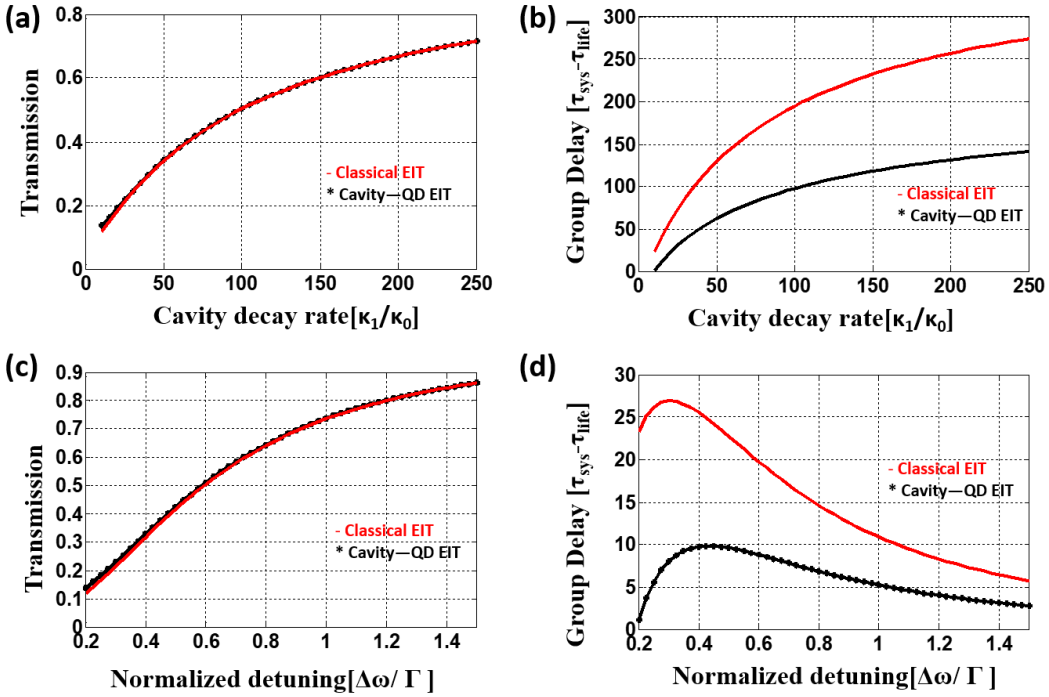

Figure 3.4. Comparison of transmission spectrum (a) and generated group delay (b) of single embedded QD in cavity and cavity-cavity array with the coupling strength of 0.2Γ. Same transmission (c) and group delay (d) graphs are repeated for $\kappa=10\kappa_0$.

In this thesis, discussed systems are the types of optical filters which result in limitation restrictions on the broadband optical delays [50]. Then bandwidth of transparency window for cavity-QD EIT and classical EIT are analyzed. Short-range optical pulses which are less than the inverse of the resonance's bandwidth is distorted at higher resonances. For this reason, higher peak values result in smaller resonance bandwidth at generated group delay.

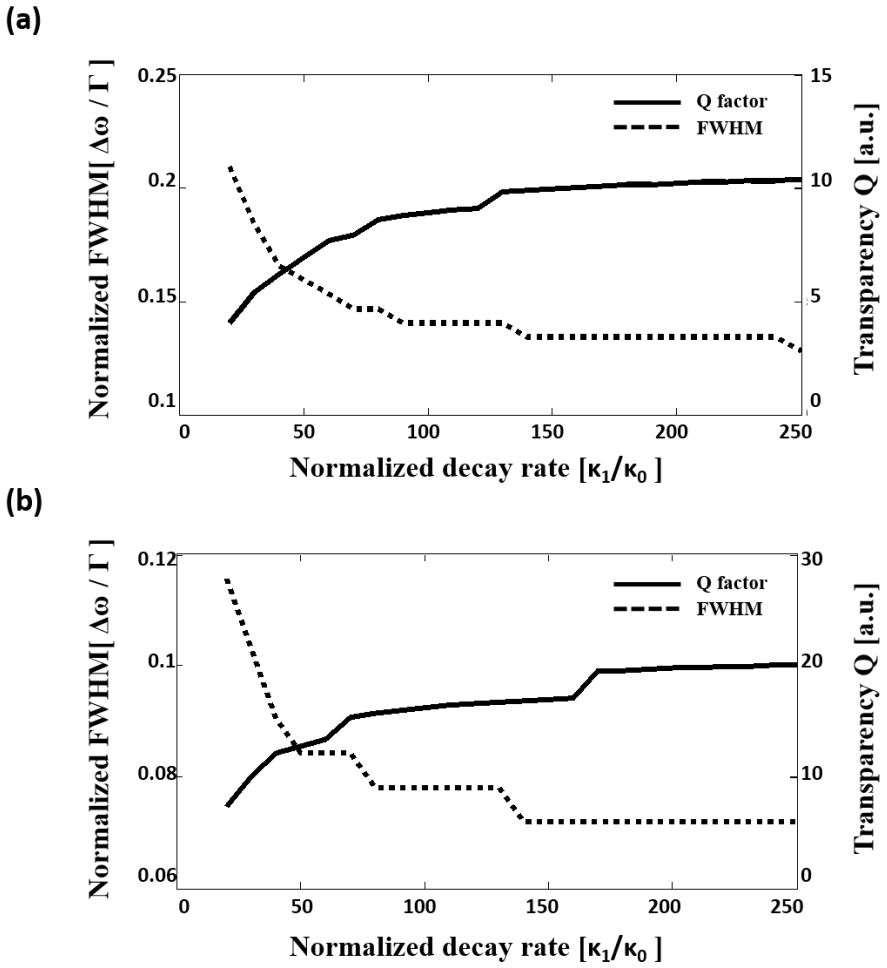

Figure 3.5. Cavity-QD EIT (a) and Classical EIT (b) bandwidth of the transparency peaks and the corresponding quality factor.

Full-Width Half-Maximum (FWHM) identifies the allowed range of light wavelength to pass through. The transmission spectrum of Figure 3.3 (c) and Figure 3.3 (d) are used to obtain full width half-maximum (FWHM) at transparency peaks. The delay-bandwidth limitation values are demonstrated in Figure 3.5. The cavity-QD [Figure 3.5 (a)] configuration has a wider bandwidth than the classical EIT [Figure 3.5 (b)] configuration leading to a lower transparency peak quality factor. In addition, when transmission peak value increases, transparency quality factors decrease.

3.2. Single QD Embedded in Cavity-Cavity Array and Triple Cavity Array

Cavity-QD EIT and classical EIT systems comparison give important results in terms of phase delay and transmission. Another comparison is made between single QD embedded in cavity-cavity array [Figure 3.6 (a)] and triple cavity array [Figure 3.6 (b)] in this part.

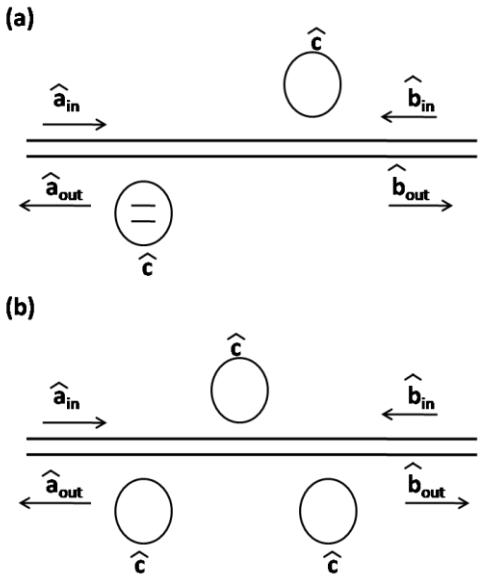

Figure 3.6. Single QD embedded in cavity-cavity array (a) and triple cavity array (b).

Equation for single quantum dot embedded in cavity-cavity array transportation equation is derived from the formula of cavity-QD EIT as follows:

$$\begin{pmatrix} \hat{b}_{in}(\omega) \\ \hat{b}_{out}(\omega) \end{pmatrix} = \frac{1}{\alpha - \Gamma + \kappa_1} \begin{pmatrix} -\kappa_1 & \alpha - \Gamma \\ \alpha - \Gamma + 2\kappa_1 & -\kappa_1 \end{pmatrix} \begin{pmatrix} 0 & e^{j2\pi} \\ e^{j2\pi} & 0 \end{pmatrix} \frac{1}{\beta - \Gamma + \kappa_2} \begin{pmatrix} -\kappa_2 & \beta - \Gamma \\ \beta - \Gamma + 2\kappa_2 & -\kappa_2 \end{pmatrix} \begin{pmatrix} \hat{a}_{in}(\omega) \\ \hat{a}_{out}(\omega) \end{pmatrix} \quad (3.12)$$

where $\alpha = i(\omega - \omega_c) + \frac{|g|^2}{i(\omega - \omega_r) - \gamma}$ and $\beta = i(\omega - \omega_c)$

Triple cavity transportation matrix is represented in Equation 3.13. Triple cavity system has no QD so $g_1 = g_2 = g_3 = 0$.

$$\begin{pmatrix} \hat{b}_{in}(\omega) \\ \hat{b}_{out}(\omega) \end{pmatrix} = \frac{1}{\beta_1 - \Gamma + \kappa_1} \begin{pmatrix} -\kappa_1 & \beta_3 - \Gamma \\ \beta_1 - \Gamma + 2\kappa_1 & -\kappa_1 \end{pmatrix} \begin{pmatrix} 0 & e^{j2\pi} \\ e^{j2\pi} & 0 \end{pmatrix} \frac{1}{\beta_2 - \Gamma + \kappa_2} \begin{pmatrix} -\kappa_2 & \beta_2 - \Gamma \\ \beta_2 - \Gamma + 2\kappa_2 & -\kappa_2 \end{pmatrix} \begin{pmatrix} 0 & e^{j2\pi} \\ e^{j2\pi} & 0 \end{pmatrix} \frac{1}{\beta_3 - \Gamma + \kappa_3} \begin{pmatrix} -\kappa_3 & \beta_3 - \Gamma \\ \beta_3 - \Gamma + 2\kappa_3 & -\kappa_3 \end{pmatrix} \begin{pmatrix} \hat{a}_{in}(\omega) \\ \hat{a}_{out}(\omega) \end{pmatrix} \quad (3.13)$$

where $\beta_j = i(\omega - \omega_j)$

In Figure 3.6, single quantum dot embedded cavity-cavity array and triple cavity array systems are compared in terms of transmission spectra, the phase of the transmitted fields and group delay ($d\phi/d\omega$) values. The transmission characteristics [Figure 3.7 (a) and Figure 3.7 (b)] and the corresponding phase/group delay values [Figure 3.7 (c) and Figure 3.7 (d)] look similar for both the single QD embedded cavity-cavity array and triple cavity array.

Figure 3.7 (b) shows the spectral transmission characteristic of the triple cavity case. The coupling strength value is assumed to be zero because the coherent interaction occurs if and only if the bus waveguide phase accumulation is an integer multiple of 2π. The group delay corresponding to calculated transmission spectra is given in Figure 3.7 (d). The resonant frequencies ($-\Delta\omega$, 0, $\Delta\omega$) are modified by varying the first and third cavity resonant frequencies. $\Delta\omega$ values are changed as 0.5Γ, 1.33Γ and 5Γ which are shown for the red, black and blue lines, respectively [Figure 3.7 (f)]. The same variation is applied to single QD embedded in cavity-cavity array [Figure 3.7 (e)].

Figure 3.7 (a) shows the spectral transmission characteristics for the case where a single QD embedded cavity-cavity array. The QD resonantly interacts with the first cavity in the presence of the QDs. The values of the intrinsic and extrinsic cavity decay rates are the same as the triple cavity case. In addition, the transition and resonant frequencies are equal.

In the following, extrinsic cavity decay rates are assumed to be the same values $\kappa_3=\kappa_2=\kappa_1=\kappa$ as a result $\Gamma_3=\Gamma_2=\Gamma_1=\Gamma$ to make the equations simpler. Total decay rate(γ) equals to κ_0 as in the previous configuration.

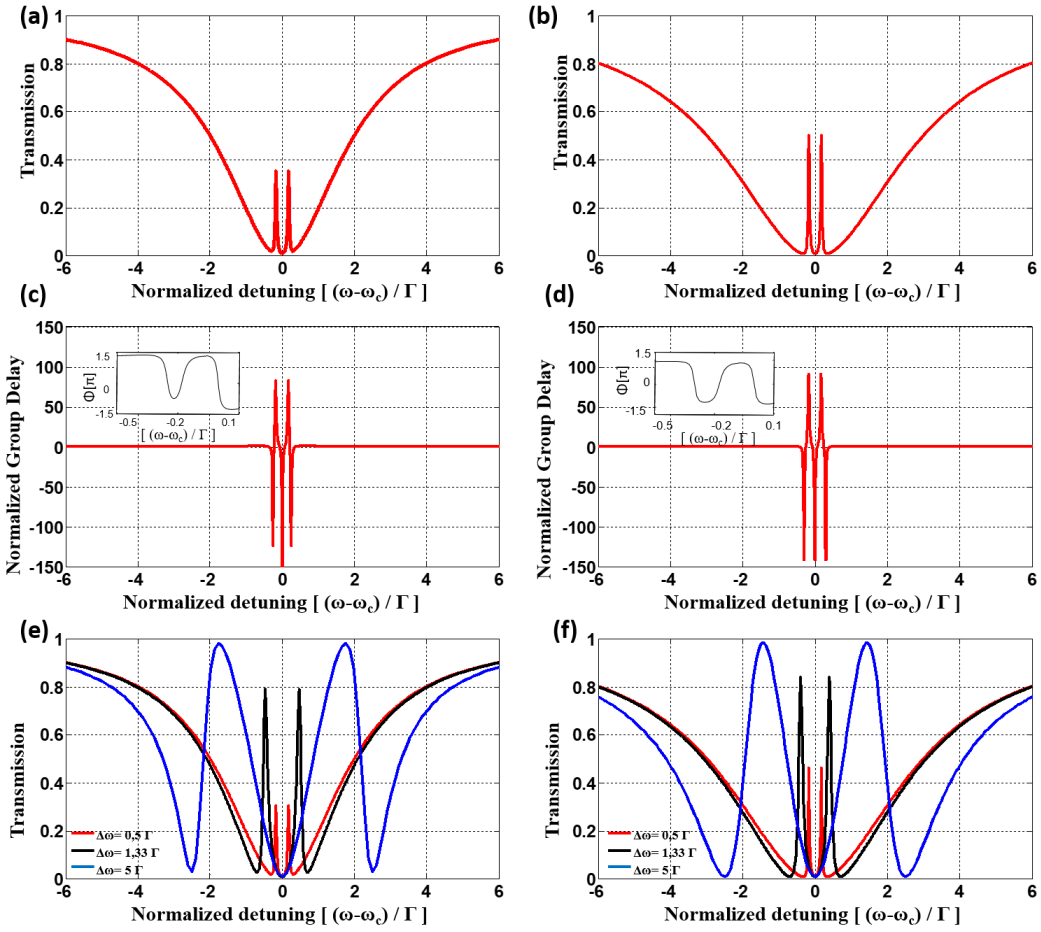

Figure 3.7. The transmission spectrum for single embedded QD in cavity-cavity array (triple cavity array) a (b). The corresponding phase and group delay c (d).Transmission variation for various detuning for single embedded QD in cavity-cavity array (triple cavity array) e (f) [9].

3.3. Spectral Character and Group Delay Comparison

Single QD embedded cavity-cavity array and triple cavity array systems transmission equations are analyzed below to compare the configurations with simulation results.

Double cavity with QD transmission Equation 3.12 transforms into:

$$\frac{\hat{b}_{out}(\omega)}{\hat{a}_{in}(\omega)} = \frac{(\kappa + \beta_2 - \Gamma).(\kappa + \beta_1 - \Gamma)}{[(\beta_1 - \Gamma)(\beta_2 - \Gamma) - \kappa^2]} \tag{3.14}$$

Triple cavity transmission Equation 3.13 transforms into:

$$\frac{\hat{b}_{out}(\omega)}{\hat{a}_{in}(\omega)} = \frac{(\kappa + (\beta_1 - \Gamma))(\kappa + (\beta_1 - \Gamma))(\kappa + (\beta_1 - \Gamma))}{(\beta_3 - \Gamma)(\beta_2 - \Gamma)(\beta_1 - \Gamma) - \kappa^2(\beta_1+\beta_2+\beta_3 - 3\Gamma) - 2\kappa^3} \tag{3.15}$$

First of all, β value is written to compare the transmission configurations. Equation 3.14 is solved for t(ω):

$$t(\omega) = \frac{\left(2\omega^2\kappa_0 - \frac{1}{2}g^2\kappa_0 - \frac{1}{4}{\kappa_0}^3\right) + i\omega\left(-\omega^2 + g^2 + \frac{5}{4}{\kappa_0}^2\right)}{\left(2\omega^2(\kappa_0 + \kappa) - g^2(\kappa - \frac{1}{2}\kappa_0) - {\kappa_0}^2(\kappa - \frac{1}{4}\kappa_0)\right) + i\omega\left(g^2 - \omega^2 + 3\kappa\kappa_0 + \frac{5}{4}{\kappa_0}^2\right)} \tag{3.16}$$

Then, similar steps are repeated for the triple cavity case and the detuning between the cavities is Δω. The transmission values are dependent to frequency spectrum and normalized group delay is shown as:

$$t(\omega) = \frac{\left(\frac{3}{2}\omega^2\kappa_0 - \frac{1}{8}{\kappa_0}^3 - \frac{1}{2}\kappa_0\Delta\omega^2\right) + i\omega\left(-\omega^2 + \frac{3}{4}{\kappa_0}^2 + \Delta\omega^2\right)}{\left(3\omega^2\kappa + \frac{3}{2}\omega^2\kappa_0 - \frac{3}{4}\kappa{\kappa_0}^2 - \frac{1}{8}{\kappa_0}^3 - \Delta\omega^2\kappa - \frac{1}{2}\kappa_0\Delta\omega^2\right) + i\omega\left(\Delta\omega^2 - \omega^2 + 3\kappa\kappa_0 + \frac{3}{4}{\kappa_0}^2\right)} \tag{3.17}$$

When the extrinsic cavity is greater than the intrinsic cavity decay rate, transmission values are shown for double cavity and triple cavity, respectively.

$$t(\omega) = \frac{\left(2\omega^2\kappa_0 - \frac{1}{2}g^2\kappa_0\right) + i\omega(-\omega^2 + g^2)}{(2\omega^2\kappa - \kappa g^2 - \kappa{\kappa_0}^2) + i\omega(-\omega^2 + g^2 + 3\kappa\kappa_0)} \tag{3.18}$$

$$t(\omega) = \frac{\left(\frac{3}{2}\omega^2\kappa_0 - \frac{1}{2}\kappa_0\Delta\omega^2\right) + i\omega(-\omega^2 + \Delta\omega^2)}{\left(3\omega^2\kappa - \Delta\omega^2\kappa - \frac{3}{4}\kappa{\kappa_0}^2\right) + i\omega(-\omega^2 + \Delta\omega^2 + 3\kappa\kappa_0)} \tag{3.19}$$

3.3.1. Simulation Results

In this study, single QD embedded cavity-cavity array and triple cavity array cases are compared with various parameters. Firstly, the extrinsic cavity decay rate, κ, values are varied from $20\kappa_0$ to $250\kappa_0$ with equal steps. Group delay and transmission spectra values are calculated for both configurations in Figure 3.8 (a) and Figure 3.8 (b). Resonant frequencies are -0.3Γ, 0 and 0.3Γ for the ω_{c1}, ω_{c2}, and ω_{c3} values, respectively. The coupling strength (g) value is set to 0.5Γ. Transmission values of the triple cavity array are higher than the single QD cavity-cavity array. As far as the group delay is considered, the triple cavity is higher than the double cavity when extrinsic cavity decay rate is smaller than the $55\kappa_0$, Beyond the $55\kappa_0$ transmission values of triple cavity is lower than the double cavity.

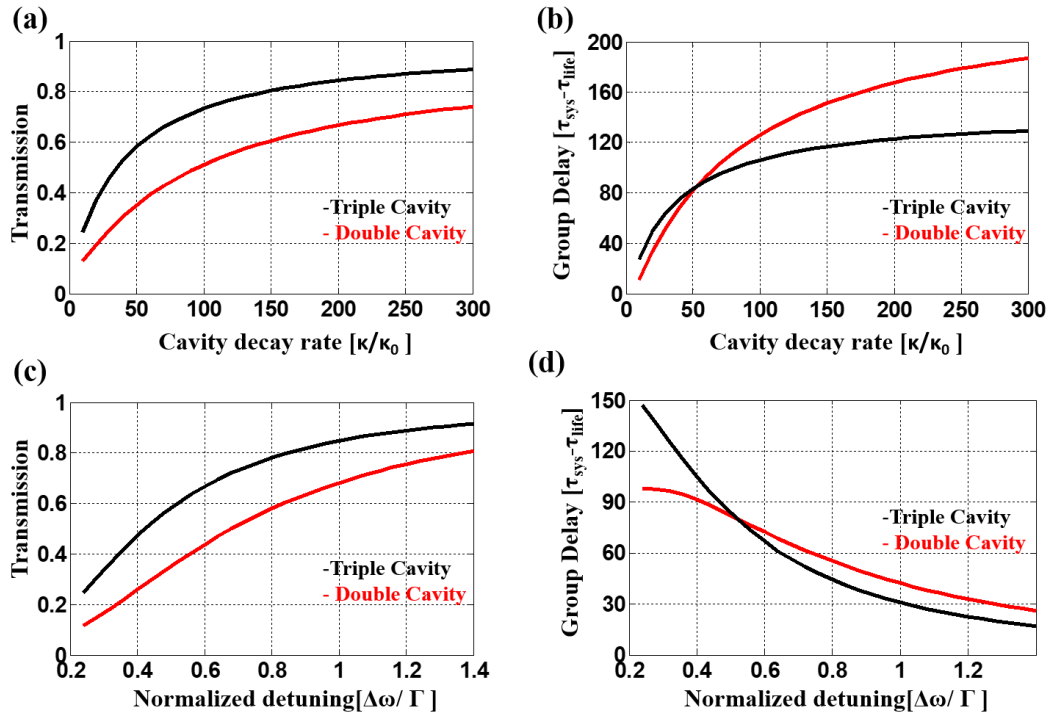

Figure 3.8. Comparison of transmission spectrum (a) and generated group delay (b) of single embedded QD in cavity-cavity array and triple cavity array with the coupling strength of 0.5Γ. Same transmission (c) and group delay (d) graphs are repeated for $\kappa=50\kappa_0$.

Then, the calculations in Figure 3.7 (a) and Figure 3.7 (b) are repeated with stationary extrinsic cavity decay rate in Figure 3.7 (c) and Figure 3.7 (d). Coupling strength values are varied from 0.2Γ to 1.4Γ with equal steps. The transmission values of triple cavity decay rates are higher than the single QD embedded in cavity-cavity array values. When the coupling strength value is nearly smaller than 0.5Γ, triple cavity group delay is higher than the single QD embedded cavity-cavity array. If we look at the higher values, triple cavity group delay values are smaller than the single QD embedded in cavity-cavity array group delay values.

Furthermore, Figure 3.7 is repeated with different values to obtain more meaningful comments about transmission and group delay comparison in Figure 3.8. Coupling strength value is set to 0.3Γ. When we look at the transmission values, both of single QD embedded cavity-cavity array and triple cavity array are smaller than in Figure 3.8 (a). Transmission values of triple cavity array are more comparable and greater than the single embedded QD cavity-cavity array in Figure 3.9 (a). Group delay intersection point is shifted to a higher normalized decay rate ($\kappa_{1/}\ \kappa_0$) in Figure 3.9 (b). Behind the intersection point, triple cavity group delay values are still higher than single QD embedded cavity-cavity array system. It is shown that decreasing the coupling strength value results in higher group delay values.

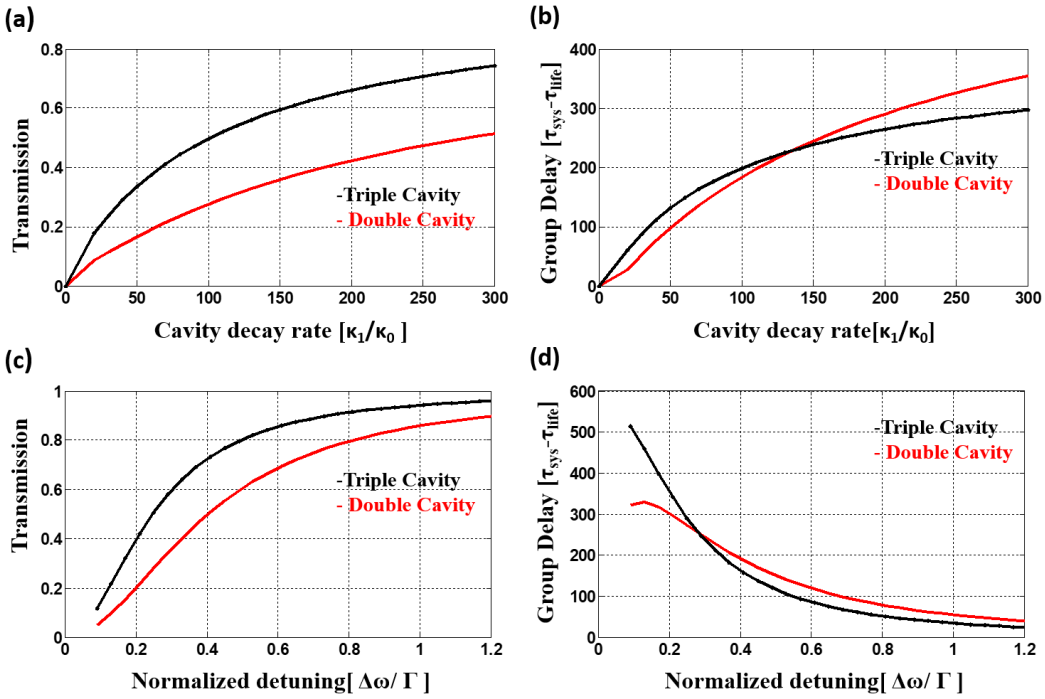

Figure 3.9. Comparison of transmission spectrum (a) and generated group delay (b) of single QD embedded in cavity-cavity array and triple cavity array with the coupling strength of 0.3Γ. Same transmission (c) and group delay (d) graphs are repeated for $\kappa=150\kappa_0$.

In Figure 3.9 (c) and Figure 3.9 (d), the extrinsic cavity decay rate is set to $150\kappa_0$. Increasing the extrinsic cavity decay rate leads to catching up the transmission difference between triple cavity array and single QD embedded cavity-cavity array at higher coupling strength values. Triple cavity array transmission values are still higher than the single QD embedded cavity-cavity array like previous examples. Both of the systems group delay values are increasing while coupling strength is increasing. On the other hand, group delay values of both systems are higher than the previous example. Group delay values of the triple cavity array are higher than the double cavity when coupling strength value is nearly 0.3Γ.

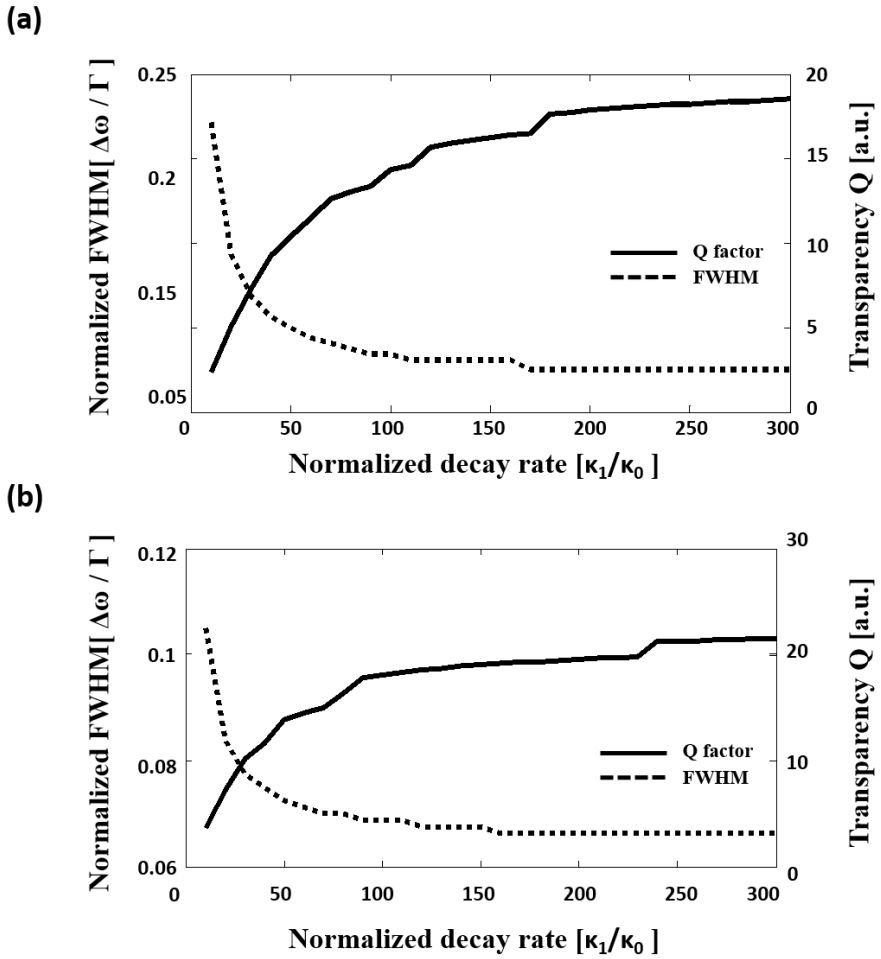

Figure 3.10. Triple cavity (a) and single embedded QD in cavity-cavity array (b) bandwidth of the transparency peaks and the corresponding quality factor

The transmission spectrum of Figure 3.9 (c) and Figure 3.9 (d) are used to obtain full width half-maximum (FWHM) at transparency peaks. The delay-bandwidth limitation values are demonstrated in Figure 3.10. Single QD embedded in cavity-cavity array [Figure 3.10 (b)] configuration has a wider bandwidth than triple cavity [Figure 3.10 (a)] configuration leading to a lower transparency peak quality factor.

While varying the extrinsic cavity decay rate and coupling strength value, there is an intersection point of group delay values. Group delay simulations are repeated at different extrinsic cavity decay rates. Then the intersection point of triple cavity and

single QD embedded cavity-cavity array are gathered and showed in Figure 3.11 separately. While extrinsic cavity decay rate is increasing, the intersection points of triple cavity and single QD embedded cavity-cavity array is decreasing. It shows us that if we increase the extrinsic cavity decay rate sufficiently, the group delay value of single QD embedded cavity-cavity is higher than the triple cavity array. When the extrinsic cavity decay rate is more comparable with intrinsic cavity decay rate, choosing the suitable system requires looking at the coupling strength values. Smaller coupling values make the group delay of the triple cavity is more effective than single QD embedded in cavity-cavity.

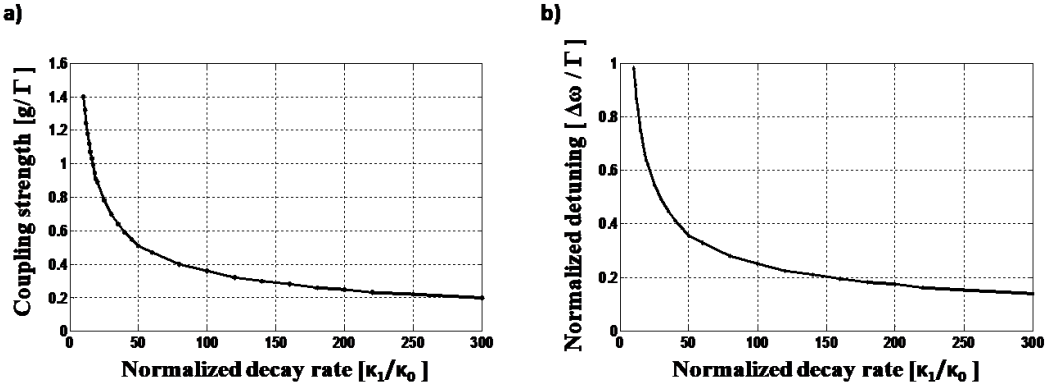

Figure 3.11. Group delay intersection values for coupling strength (a) and normalized detuning (b)

Group delay intersection values are found by varying extrinsic cavity decay rate from $20\kappa_0$ to $300\kappa_0$ in Figure 3.11. Under the intersection line, triple cavity group delay values are higher than single QD embedded cavity-cavity array. Moreover, triple cavity systems have larger coupling strength scale at low extrinsic cavity decay rates. On the other hand, when we increase the extrinsic cavity decay rate, triple cavity phase delay is higher than single QD embedded cavity-cavity array only for coupling strength values smaller than about 0.2Γ.

Furthermore, single QD embedded cavity-cavity array and triple cavity array subsystems analyzed above are simulated again in case the various parameters are tuned. Firstly, the extrinsic cavity decay rate (κ) value is varied from $20\kappa_0$ to $250\kappa_0$ with equal steps and the group delay and transmission spectra values are calculated for both configurations. In Figure 3.12 (a) where the resonant frequencies are -0.7Γ, 0 and 0.7Γ for the ω_{c1}, ω_{c2} and ω_{c3} respectively and the coupling strength (g) value is set to 0.7Γ. Transmission values of the triple cavity and single QD embedded in cavity-cavity array systems are equal to each other at especially high extrinsic cavity decay rates. As far as the group delay is considered, the results are quite interesting. As can be seen in Figure 3.12 (b), triple cavity system generates higher group delay values than single QD embedded cavity-cavity array system.

Then, frequency detuning dependency of the spectral characteristics has also been analyzed. This detuning corresponds to the frequency spacing between different channels in the WDM systems. Frequency splitting in the transmission spectrum comes from the coupling strength between the QD and the cavities in the quantum dot embedded double cavity system and from the resonant frequency difference in the triple cavity array system. When the coupling strength changes, normalized detuning values differ with the same rate in the triple cavity array system. This tuning has been scanned from 0.2Γ to 1.4Γ and the results have been summarized in Figure 3.12 (c) and Figure 3.12 (d). The transmission values are increasing and the generated group delay is decreasing with increasing frequency detuning as expected from the fact that the delay-bandwidth product is constant unless there is a dynamical tuning [26]. In terms of the propagation delay value, triple cavity phase delay values are higher than the single QD embedded cavity-cavity array system.

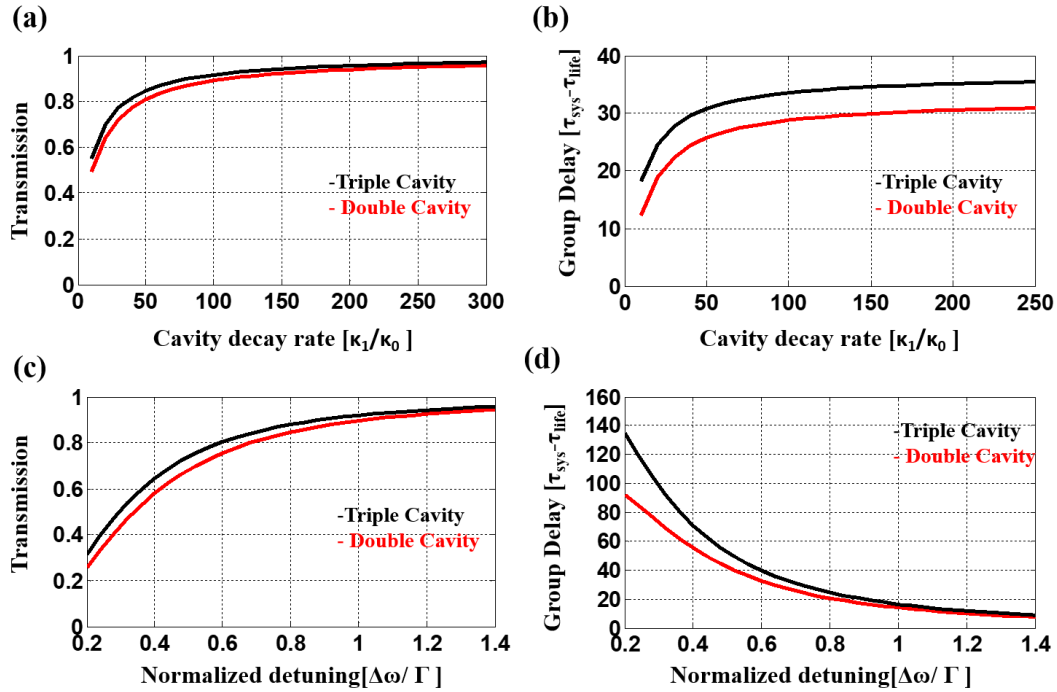

Figure 3.12. Comparison of transmission spectrum (a) and generated group delay (b) of single embedded QD in cavity-cavity array and triple cavity array with the coupling strength of 0.7Γ. Same transmission (c) and group delay (d) graphs are repeated for $\kappa=50\kappa_0$ [9]

Next, the calculations in Figure 3.12 are repeated for a different set of parameters. In particular, extrinsic cavity decay rate scan has been run with a smaller detuning ($g = 0.3\Gamma$ and $\Delta\omega= 0.3\Gamma$) values and the results are shown in Figure 3.13. The observed characteristics are still present previous characteristic but the exact values have been changed. Triple cavity transmission and phase delay values are still higher than single QD embedded cavity-cavity array system. On the other hand, smaller detuning results in higher phase delay values [Figure 3.13 (b)]. At the lower rate of extrinsic cavity decay rates, phase delay values are decreased quietly in Figure 3.13 (d).

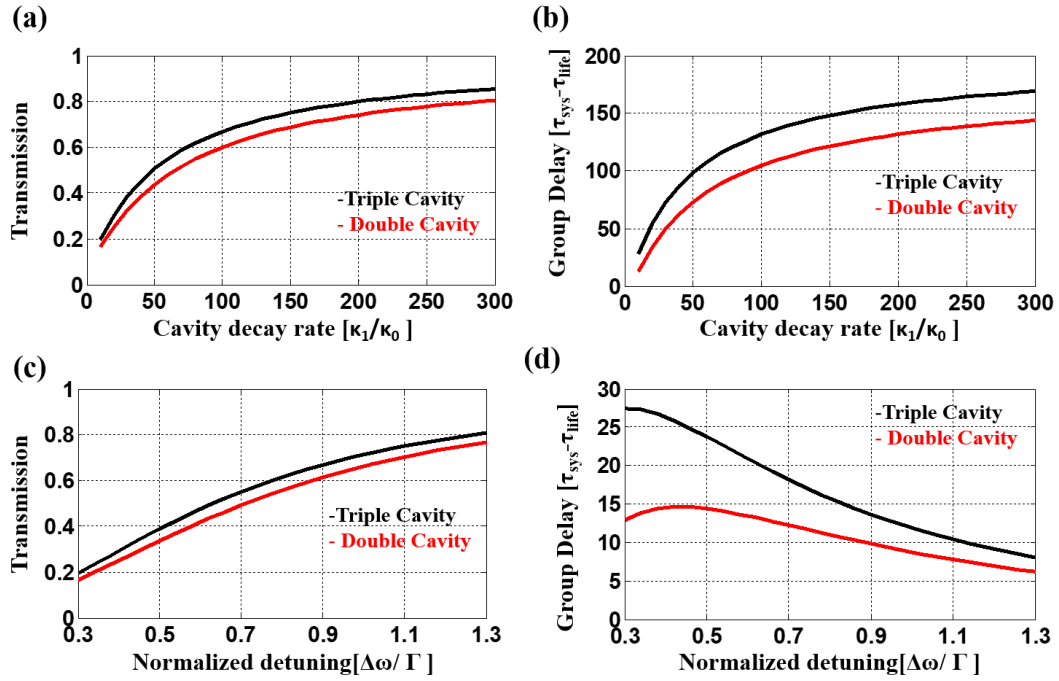

Figure 3.13. Comparison of transmission spectrum (a) and generated group delay (b) of single embedded QD in cavity-cavity array and triple cavity array with the coupling strength of 0.3Γ. Same transmission (c) and group delay (d) graphs are repeated for $\kappa=10\kappa_0$ [9]

Transmission values are calculated by using Equation 3.18 and Equation 3.19. Single QD embedded cavity-cavity array is calculated when coupling strength value is set to 0.5Γ and $\omega_1=0.35\Gamma$. Transmission calculations are shown in Equation 3.20 and Equation 3.21.

$$\frac{\kappa_0(2(0.35\Gamma)^2-0.5(0.5\Gamma)^2)+i0.35\Gamma((0.5\Gamma)^2-(0.35\Gamma)^2)}{\kappa(2(0.35\Gamma)^2-(0.5\Gamma)^2)+i0.35\Gamma((0.5\Gamma)^2-(0.35\Gamma)^2+3\kappa\kappa_0)} \quad (3.20)$$

$$t(\omega 1=0.35\Gamma)=\frac{0.12\Gamma^2\kappa_0+i0.04625\Gamma^3}{-0.005\Gamma^2\kappa+i(0.04625\Gamma^3+1.05\Gamma\kappa\kappa_0)} \quad (3.21)$$

Triple cavity array is calculated when coupling strength value is set to 0.5Γ and $\omega_2=0.2875\Gamma$. The transmission calculations are shown in Equation 3.22 and Equation 3.23.

$$t(\omega) = \frac{(1.5(0.2875\Gamma)^2\kappa_0 - 0.5(0.5\Gamma)^2\kappa_0) + i0.2875\Gamma\left((0.5\Gamma)^2 - (0.2875\Gamma)^2\right)}{(3\kappa(0.2875\Gamma)^2 - \kappa(0.5\Gamma)^2) + i0.2875\Gamma\left((0.5\Gamma)^2 - (0.2875\Gamma)^2 + 3\kappa\kappa_0\right)} \quad (3.22)$$

$$t(\omega 2 = 0.2875\Gamma) = \frac{-0.00101563\Gamma^2\kappa_0 + i0.04811133\Gamma^3}{-0.0020313\Gamma^2\kappa + i(0.04811133\Gamma^3 + 1.05\Gamma\kappa\kappa_0)} \quad (3.23)$$

Then calculated transmission equations are showed in Equation 3.21 and Equation 3.23 are used to find the transmission rates. Transmission rate is used to represent triple cavity transmission value to single QD embedded cavity-cavity array. While increasing the extrinsic cavity rate, the transmission rate is getting closer to each other. If we observe the transmission graphs on Figure 3.12, transmission values converge to each other at higher extrinsic cavity decay rates. It proves that simulation results and calculations are matched up with each other.

Table 3.1. *Transmission rate of triple cavity to single QD embedded cavity-cavity*

K1	**Transmission rate**	**K1**	**Transmission rate**	**K1**	**Transmission rate**
10K0	1.1144	**110K0**	1.0435	**210K0**	1.0259
20K0	1.1207	**120K0**	1.0406	**220K0**	1.0250
30K0	1.1033	**130K0**	1.0381	**230K0**	1.0241
40K0	1.0885	**140K0**	1.0360	**240K0**	1.0233
50K0	1.0771	**150K0**	1.0340	**250K0**	1.0225
60K0	1.0682	**160K0**	1.0323	**260K0**	1.0218
70K0	1.0612	**170K0**	1.0308	**270K0**	1.0212
80K0	1.0555	**180K0**	1.0294	**280K0**	1.0206
90K0	1.0508	**190K0**	1.0281	**290K0**	1.0200
100K0	1.0468	**200K0**	1.0270	**300K0**	1.0195

Transparency and normalized FWHM values of Figure 3.13 (c) and Figure 3.3 (d) are represented in Figure 3.14.

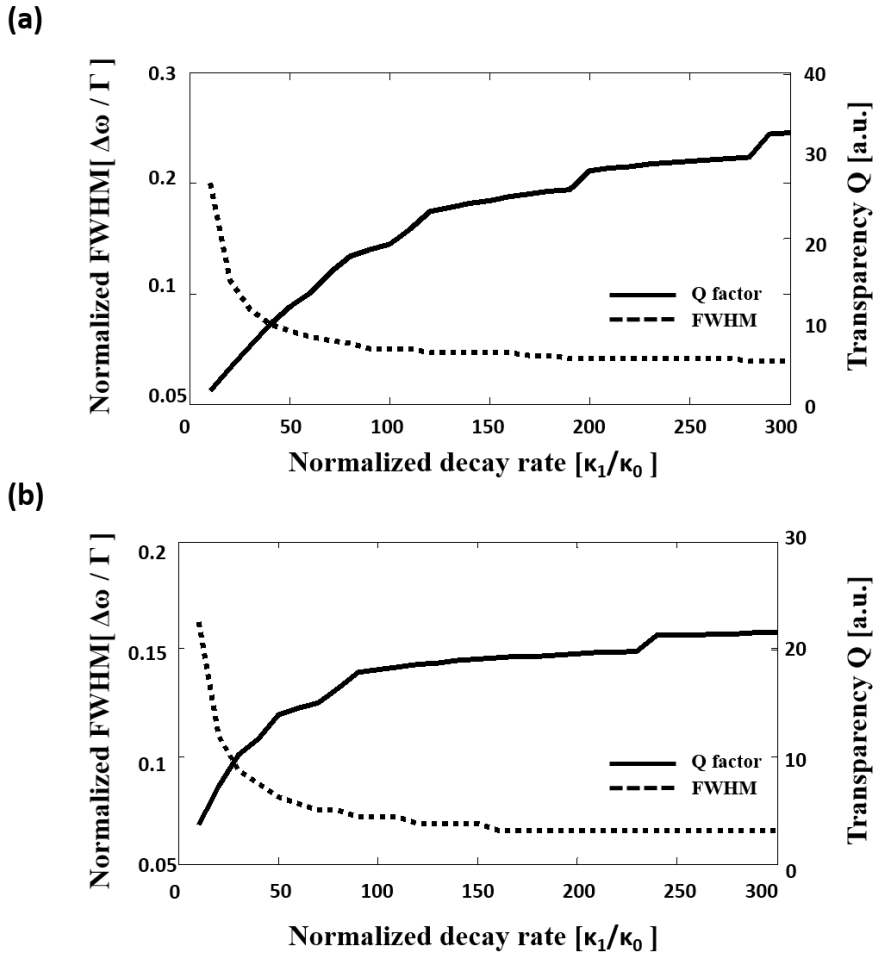

Figure 3.14. Triple cavity (a) and single QD embedded in cavity-cavity array (b) bandwidth of the transparency peaks and the corresponding quality factor

The transmission spectrum of Figure 3.12 (c) and Figure 3.12 (d) are used to obtain full width half-maximum (FWHM) at transparency peaks. The delay-bandwidth limitation values are demonstrated in Figure 3.14. Triple cavity [Figure 3.14 (a)] configuration has a wider bandwidth than single QD embedded in cavity-cavity array [Figure 3.14 (b)] configuration leading to a lower transparency peak quality factor.

3.4. Results

In summary, single embedded QD cavity-cavity array under weak coupling regime and triple cavity array systems are compared in terms of transmission spectrum and generated temporal group delay. When the extrinsic cavity decay rate is quite higher than the intrinsic cavity decay rate, the transmission values are converging to each other in case the coupling strength and the frequency detuning are equal to each other. In addition, triple cavity phase delay is higher than the single embedded QD cavity-cavity array. Higher extrinsic cavity decay rates and smaller coupling strength values result in higher phase delay values. Furthermore, if we choose the coupling strength values and normalized detuning values to get the maximum transmission values at the same frequency, transmission values of triple cavity are higher than single embedded QD in cavity-cavity array and there is an intersection point in terms of the propagation delay where the higher group delay system changes as the coupling strengths and extrinsic cavity decay rates vary. Therefore, both systems can be preferable for supplying group delays for the on-chip WDM applications depending on the component parameters.

CHAPTER 4

CONCLUSION AND FURTHER WORK

In this thesis work, single QD embedded cavity-cavity array and triple cavity array subsystems are compared in terms of transmission, phase delay, quality factor, and FWHM. The simulation results are proved with the equations which are derived from Hamiltonian dynamics and motion equations. The results showed that triple cavity array phase delay values and quality factor are higher than single QD embedded in cavity-cavity array at comparable higher extrinsic cavity decay rates.

The aim of this comparison is to answer the question that how can we apply quantum communication basic principles to classical communication applications for WDM theory. When the system has smaller FWHM, it is possible to increase the number of the signals maintained in the same fiber cable. Demand on network capacity is growing faster day by day so WDM cost-effective applications give an opportunity to researchers for higher data transmission ability.

REFERENCES

[1] M. V. V. and S. D. I. and V. N. Z., *Quantum Mechanics for Nanostructures*, First. Cambridge: Cambridge University Press, 2010.

[2] S. K. Subedi, "An introduction to nanotechnology and its implications," pp. 78–81, 1985.

[3] C. J. Chen, "Introduction to Scanning Tunneling Microscopy Second Edition."

[4] A. Nouailhat, *An Introduction to Nanoscience and Nanotechnology*. .

[5] A. Stute, "A light-matter quantum interface : ion-photon entanglement and state mapping," 2012.

[6] S. M. Dutra, "Cavity quantum electrodynamics." 2005.

[7] R. J. Buenker, "Reevaluating Newton ' s Theory of Light," vol. 2, no. 6, pp. 103–110, 2015.

[8] H. J. Kimble, "Strong Interactions of Single Atoms and Photons in Cavity QED," 1998.

[9] H. Erdinç and S. Kocaman, "Analysis of quantum-dot-embedded multicavity arrays for on-chip WDM," pp. 356–367, 2018.

[10] Y. Ghasemi, P. Peymani, and S. Afifi, "Quantum dot : magic nanoparticle for imaging , detection and targeting," pp. 156–165, 2009.

[11] T. Hayashi, T. Fujisawa, H. D. Cheong, Y. H. Jeong, and Y. Hirayama, "Coherent manipulation of electronic states in a double quantum dot," pp. 1–5, 2008.

[12] A. Majumdar, "Solid state cavity QED with quantum dots coupled to photonic crystal cavities," no. July, 2012.

[13] P. Michler, *Single Quantum Dots Fundamentals, Applications and New Concepts*. Springer, 2003.

[14] V. I. Klimov, "Nanocrystal Quantum Dots From fundamental photophysics to multicolor lasing," no. 28, pp. 214–220, 2003.

[15] T. Chakraborty, "Quantum dots." Elsevier, 1999.

[16] J. Chen, V. Hardev, and J. Yurek, "Quantum-dot displays: Giving LCDs a competitive edge through color," *Inf. Disp. (1975).*, vol. 29, no. 1, pp. 12–17, 2013.

[17] R. Hanson, L. P. Kouwenhoven, J. R. Petta, S. Tarucha, and L. M. K. Vandersypen, “Spins in few-electron quantum dots,” vol. 79, no. December, pp. 1217–1265, 2007.

[18] A. Fuhrer and C. Fasth, “Coulomb blockade in Quantum Dots Cg,” pp. 1–16, 2007.

[19] M. Yadav and A. Chaudhary, “Quantum Dots : An Introduction,” *Int. J. Res. Advent Technol.*, no. Special Issue, pp. 61–66, 2014.

[20] E. O. Chukwuocha, M. C. Onyeaju, and T. S. T. Harry, “Theoretical Studies on the Effect of Confinement on Quantum Dots Using the Brus Equation,” vol. 2012, no. May, pp. 96–100, 2012.

[21] W. C. G., “OPTICAL CAVITY PHYSICS,” pp. 1–9, 2017.

[22] D. A. Steck, *Classical and Modern Optics*. .

[23] K. D.J., “Introduction to Semiconductor Lasers for Optical Communications,” New York, NY: Springer, 2014, pp. 1–21.

[24] J. D. Joannopoulos, S. G. Johnson, J. N. Winn, and R. D. Meade, *Photonic Crystals: Molding the Flow of Light*, Second. Princeton University Press, 2008.

[25] Z. Bushell, M. Florescu, and S. Sweeney, “High-Q photonic crystal cavities in all-semiconductor photonic-crystal heterostructures,” vol. 1, no. d, pp. 1–5, 2017.

[26] S. G. Carter *et al.*, “Photonic Crystal Cavity,” *Nature Photonics*, 2013. [Online]. Available: http://dx.doi.org/10.1038/nphoton.2013.41.

[27] E. Purcell, H. Torrey, and R. Pound, “Resonance Absorption by Nuclear Magnetic Moments in a Solid,” *Phys. Rev.*, vol. 69, no. 1–2, pp. 37–38, 1946.

[28] P. Lodahl, I. S. Nikolaev, A. F. Van Driel, and W. L. Vos, “Dynamics of spontaneous emission controlled by local density of states in photonic crystals,” *Conf. Lasers Electro-Optics 2006 Quantum Electron. Laser Sci. Conf. CLEO/QELS 2006*, 2006.

[29] P. Related, “Reports on Progress in Physics Related content Fundamental quantum optics in structured reservoirs,” 2000.

[30] K. Semba, “Selected Papers : Quantum Computing Entanglement Control of Superconducting Qubit Single Photon System.”

[31] S. E. Morin, Q. Wu, and T. W. Mossberg, “CAVITY QUANTUM ELECTRODYNAMICS AT OPTICAL FREQUENCIES,” pp. 10–13.

[32] D. Englund, A. Faraon, I. Fushman, N. Stoltz, P. Petroff, and J. Vuc,

"Controlling cavity reflectivity with a single quantum dot," vol. 450, no. December, pp. 857–861, 2007.

[33] T. P. Spiller, "Quantum information technology," *Mater. Today*, vol. 6, no. 1, pp. 30–36, 2003.

[34] T. P. Spiller, "Basic elements of quantum information technology," 1997.

[35] S. Muralidharan, L. Li, J. Kim, N. Lütkenhaus, M. D. Lukin, and L. Jiang, "Optimal architectures for long distance quantum communication," *Sci. Rep.*, vol. 6, no. 1, p. 20463, 2016.

[36] S. E. Vinay and P. Kok, "Practical Repeaters for Ultra-Long Distance Quantum Communication," pp. 1–8, 2017.

[37] V. Ii, I. M. F. By, and I. M. F. By, "Observation of entanglement between a single trapped atom and a single photon," *Nature*, vol. 432, no. November, pp. 81–84, 2004.

[38] K. Azuma, K. Tamaki, and H.-K. Lo, "All-photonic quantum repeaters," *Nat. Commun.*, vol. 6, p. 6787, 2015.

[39] B. R. Sletteng and N. E. Asa, "Wavelength Division Multiplexing - an overview .," *Architecture*, vol. 4, no. 5, pp. 1–4, 2002.

[40] "DWDM over CWDM network - PacketLight Networks." [Online]. Available: https://www.packetlight.com/innovations/dwdm-over-cwdm-network. [Accessed: 17-Feb-2018].

[41] "Differences between CWDM and DWDM - Fiber Optic ComponentsFiber Optic Components." [Online]. Available: http://www.fiber-optic-components.com/differences-between-cwdm-and-dwdm-2.html. [Accessed: 17-Feb-2018].

[42] A. Zhu, "How to Use WDM for Fiber Capacity Expansion," *Fiber Optic Solution*. [Online]. Available: http://www.fiber-optic-solutions.com/use-wdm-fiber-capacity-expansion.html.

[43] F. Grusdt, "Introduction to Cavity QED," no. 6, pp. 1–8, 2011.

[44] J. D. Cresser, "Quantum Physics Notes," vol. 2, no. August, 2011.

[45] F. J. Garc, L. Mart, and D. Zueco, "Weak and Strong coupling regimes in plasmonic-QED," pp. 1–18.

[46] E. Waks and J. Vuckovic, "Dipole induced transparency in drop-filter cavity-waveguide systems," *Phys. Rev. Lett.*, vol. 96, no. 15, pp. 1–4, 2006.

[47] I. Fushman, "QUANTUM DOTS IN PHOTONIC CRYSTALS: FROM QUANTUM INFORMATION PROCESSING TO SINGLE PHOTON

NONLINEAR OPTICS," no. December, 2008.

[48] K. J. Vahala, "Optical microcavities," vol. 424, no. August, pp. 839–846, 2004.

[49] I. Fushman, D. Englund, A. Faraon, and J. Vuckovic, "Probing the interaction between a single quantum dot and photonic crystal cavity," *Phys. Status Solidi*, vol. 2815, no. 9, pp. 2808–2815, 2008.

[50] J. Vuckovic, D. Englund, A. Faraon, I. Fushman, and E. Waks, "Quantum Information Processing with Quantum Dots in Photonic Crystals," *Semicond. Quantum Bits*, pp. 423–452, 2008.

[51] S. Kocaman and G. Turhan Sayan, "Comparision of coherently coupled multi-cavity and quantum dot embedded single cavity systems," *Opt. Express*, vol. 24, 2016.

[52] P. Vasa and C. Lienau, "Strong Light-Matter Interaction in Quantum Emitter / Metal Hybrid Perspective Strong Light-Matter Interaction in Quantum Emitter / Metal Hybrid Nanostructures," no. October, 2017.

[53] N. Caselli, F. Riboli, A. Gerardino, and L. Li, "Tailoring the photon hopping by nearest and next-nearest- neighbour interaction in photonic arrays."

[54] Y. F. Xiao *et al.*, "Coupled quantum electrodynamics in photonic crystal cavities towards controlled phase gate operations," *New J. Phys.*, vol. 10, 2008.

[55] A. J. Olson and S. K. Mayer, "Electromagnetically induced transparency in rubidium," no. October 2008, pp. 116–121, 2009.

[56] S. E. Harris, "Electromagnetically Induced Transparency," *Physics Today*. pp. 36–42, 1997.

[57] S. Harris, "Electromagnetically Induced Transparency," *Phys. Today*, vol. 50, no. Cm, p. 36, 1997.

[58] X. Zhou, L. Zhang, W. Pang, H. Zhang, Q. Yang, and D. Zhang, "Phase characteristics of an electromagnetically induced transparency analogue in coupled resonant systems," *New J. Phys.*, vol. 15, 2013.

[59] L. V. Hau, S. E. Harris, Z. Dutton, C. H. Behroozi, and E. H. L. Boulevard, "Light speed reduction to 17 metres per second in an ultracold atomic gas," vol. 397, no. February, pp. 594–598, 1999.

[60] H. P. Specht, N. Christian, A. Reiserer, E. Figueroa, S. Ritter, and G. Rempe, "A Single-Atom Quantum Memory."

APPENDICES

A. Cavity-QD EIT

$$\frac{\hat{b}_{out}}{\hat{a}_{in}} = m * \hat{a}_{out} = \hat{b}_{in} - \sqrt{\kappa_1}\hat{c}$$

$$\hat{b}_{out} = \hat{a}_{in} - \sqrt{\kappa_1}\hat{c}$$

$$\frac{d\hat{c}}{dt} = -i[\hat{c}, H] - \Gamma\hat{c} + \sqrt{\kappa_1}(\hat{a}_{in} + \hat{b}_{in})$$

$$\frac{d\hat{\sigma}_-}{dt} = -i[\hat{\sigma}_-, H] - \gamma\hat{\sigma}_- + \sqrt{\bar{\gamma}}\hat{\delta}$$

$$H = \omega_c\hat{c}^\dagger\hat{c} + \omega_r\hat{\sigma}_- + [g\hat{\sigma}_-\hat{c} + hc]$$

$$\hat{b}_{in}(\omega) = \left(\frac{\kappa_1}{-\alpha + \Gamma - \kappa_1}\right)\hat{a}_{in}(\omega) + \left(\frac{-\alpha + \Gamma}{-\alpha + \Gamma - \kappa_1}\right)\hat{a}_{out}(\omega)$$

$$\hat{b}_{out}(\omega) = \left(\frac{\alpha - \Gamma + 2\kappa_1}{\alpha - \Gamma + \kappa_1}\right)\hat{a}_{in}(\omega) + \left(\frac{\kappa_1}{-\alpha + \Gamma + \kappa_1}\right)\hat{a}_{out}(\omega)$$

$$\alpha = i(\omega - \omega_c) + \frac{|g|^2}{i(\omega - \omega_r) - \gamma} = i\omega + \frac{|g|^2}{i\omega - \gamma}$$

$$\begin{pmatrix}\hat{b}_{in}(\omega)\\ \hat{b}_{out}(\omega)\end{pmatrix} = \frac{1}{\alpha - \Gamma + \kappa_1}\begin{pmatrix}-\kappa_1 & \alpha - \Gamma\\ \alpha - \Gamma + 2\kappa_1 & -\kappa_1\end{pmatrix}\begin{pmatrix}\hat{a}_{in}(\omega)\\ \hat{a}_{out}(\omega)\end{pmatrix}$$

$$\hat{b}_{in}(\omega) = 0$$

$$\hat{a}_{out} = \frac{\kappa_1}{\alpha - \Gamma}$$

$$\frac{\hat{b}_{out}}{\hat{a}_{in}} = \frac{\alpha - \Gamma + 2\kappa_1}{\alpha - \Gamma + \kappa_1} + \left(\frac{\kappa_1}{\alpha - \Gamma}\right)\left(\frac{\kappa_1}{\alpha + \Gamma + \kappa_1}\right) = \frac{\alpha - \Gamma + 2\kappa_1}{\alpha - \Gamma + \kappa_1} + \frac{{\kappa_1}^2}{(\alpha - \Gamma)(\alpha + \Gamma + \kappa_1)}$$

$$= \frac{\alpha + \kappa_1 - 0.5\kappa_0}{\alpha - 0.5\kappa_0} + \frac{{\kappa_1}^2}{(\alpha - \kappa_1 - 0.5\kappa_0)(\alpha - 0.5\kappa_0)}$$

$$\frac{\hat{b}_{out}}{\hat{a}_{in}} = \frac{\alpha - 0.5\kappa_0}{\alpha - \kappa_1 - 0.5\kappa_0}$$

$$\begin{pmatrix} \hat{b}_{in}(\omega) \\ \hat{b}_{out}(\omega) \end{pmatrix} = \frac{1}{m}\begin{pmatrix} a & b \\ c & d \end{pmatrix}\begin{pmatrix} \hat{a}_{in}(\omega) \\ \hat{a}_{out}(\omega) \end{pmatrix}$$

$$\frac{\hat{b}_{out}}{\hat{a}_{in}} = \frac{1}{m}\left(\frac{cb - da}{b}\right)$$

$$t(w) = \frac{i\omega + \frac{|g|^2}{i\omega - \gamma} - 0.5\kappa_0}{i\omega + \frac{|g|^2}{i\omega - \gamma} - \kappa_1 - 0.5\kappa_0} = \frac{\omega^2 - g^2 - \frac{\gamma\kappa_0}{2} + i\omega\left(\gamma + \frac{\kappa_0}{2}\right)}{\omega^2 - g^2 - \frac{\gamma\kappa_0}{2} - \gamma\kappa_1 + i\omega\left(\gamma + \frac{\kappa_0}{2} + \kappa_1\right)}$$

$$t(\omega = 0) = \frac{g^2 + \frac{\gamma\kappa_0}{2}}{g^2 + \frac{\gamma\kappa_0}{2} + \gamma\kappa_1} \qquad \frac{\tau_c}{\tau_{life}}(\omega = 0) = \frac{\kappa(g^2 - \gamma^2)(2\kappa + \kappa_0)}{\left(g^2 + \frac{\kappa\kappa_0}{2} + \kappa\gamma\right)\left(g^2 + \frac{\kappa\kappa_0}{2}\right)}$$

B. Classical EIT

$$\begin{pmatrix} \hat{b}_{in}(\omega) \\ \hat{b}_{out}(\omega) \end{pmatrix} = \frac{1}{\beta_2 - \Gamma + \kappa_2} \begin{pmatrix} -\kappa_2 & \beta_2 - \Gamma \\ \beta_2 - \Gamma + 2\kappa_2 & -\kappa_2 \end{pmatrix} \begin{pmatrix} 0 & e^{j2\pi} \\ e^{j2\pi} & 0 \end{pmatrix} \frac{1}{\beta_1 - \Gamma + \kappa_1} \begin{pmatrix} -\kappa_1 & \beta_1 - \Gamma \\ \beta_1 - \Gamma + 2\kappa_1 & -\kappa_1 \end{pmatrix} \begin{pmatrix} \hat{a}_{in}(w) \\ \hat{a}_{out}(w) \end{pmatrix}$$

$$m = \frac{1}{\beta_2 - \Gamma + \kappa_2} * \frac{1}{\beta_2 - \Gamma + \kappa_2}$$

$$\begin{pmatrix} \hat{b}_{in}(\omega) \\ \hat{b}_{out}(\omega) \end{pmatrix} = m \begin{pmatrix} \beta_2 - \Gamma & -\kappa_2 \\ -\kappa_2 & \beta_2 - \Gamma + 2\kappa_2 \end{pmatrix} \begin{pmatrix} -\kappa_1 & \beta_1 - \Gamma \\ \beta_1 - \Gamma + 2\kappa_1 & -\kappa_1 \end{pmatrix} \begin{pmatrix} \hat{a}_{in}(w) \\ \hat{a}_{out}(w) \end{pmatrix}$$

$$\begin{pmatrix} \hat{b}_{in}(\omega) \\ \hat{b}_{out}(\omega) \end{pmatrix} = m \begin{pmatrix} -\kappa_1 * (\beta_2 - \Gamma) - \kappa_2 * (\beta_1 - \Gamma + 2\kappa_1) & (\beta_2 - \Gamma) * (\beta_1 - \Gamma) - \kappa_2\kappa_1 \\ -\kappa_2\kappa_1 + (\beta_1 - \Gamma + 2\kappa_1) * (\beta_2 - \Gamma + 2\kappa_1) & \kappa_2 * (\beta_2 - \Gamma) + \kappa_1 * (\beta_2 - \Gamma + 2\kappa_2) \end{pmatrix} \begin{pmatrix} \hat{a}_{in}(w) \\ \hat{a}_{out}(w) \end{pmatrix}$$

$$\omega_{c1,2} = \pm \frac{\Delta\omega}{2}$$

$$g_1 = g_2 = 0$$

$$\beta_1 = i\left(w - \frac{\Delta\omega}{2}\right) \qquad \beta_2 = i\left(w + \frac{\Delta\omega}{2}\right)$$

$$\frac{\hat{b}_{out}}{\hat{a}_{in}} = \frac{\kappa^2 + \Gamma^2 - 2\kappa\Gamma - \omega^2 + \frac{\Delta\omega^2}{4} + i2\omega(\kappa - \Gamma)}{\omega^2 - \kappa^2 + \Gamma^2 + \frac{\Delta\omega^2}{4} + i2\Gamma\omega} = \frac{a + bi}{c + di} = \frac{1}{c^2 + d^2}(ac + db + i(bc - da)) = x + yi$$

if trans$= x + yi$

$\theta = \tan^{-1}(y/x)$

$$\frac{d}{d\omega}(\theta) = \frac{d}{d\omega}\left(\tan^{-1}(y/x)\right) = \frac{\left(y/x\right)'}{1 + \left(y/x\right)^2} = \frac{y'x - x'y}{y^2 + x^2}$$

$$\frac{\tau_c}{\tau_{life}}(\omega = 0) = 2\Gamma\frac{d}{d\omega}(\theta) = 2\Gamma\left(\frac{y'(\omega = 0)x(\omega = 0) - x'(\omega = 0)y(\omega = 0)}{y(\omega = 0)^2 + x(\omega = 0)^2}\right)$$

$$\theta = \tan^{-1}(y/x) = \tan^{-1}\left(\frac{\left(2\omega(\kappa - \Gamma)\right)\left(\omega^2 - \kappa^2 + \Gamma^2 + \frac{\Delta\omega^2}{4}\right) - (2\Gamma\omega)(\kappa^2 + \Gamma^2 - 2\kappa\Gamma - \omega^2 + \frac{\Delta\omega^2}{4})}{\left(\kappa^2 + \Gamma^2 - 2\kappa\Gamma - \omega^2 + \frac{\Delta\omega^2}{4}\right)\left(\omega^2 - \kappa^2 + \Gamma^2 + \frac{\Delta\omega^2}{4}\right) + (2\Gamma\omega)(2\omega(\kappa - \Gamma))}\right)$$

$$\frac{\tau_c}{\tau_{life}}(\omega = 0) = \frac{\kappa\left(\frac{\Delta\omega^2}{4} - \frac{{\kappa_0}^2}{2}\right)}{\left(\frac{\Delta\omega^2}{4} - \frac{{\kappa_0}^2}{4}\right)\left(\frac{\Delta\omega^2}{4} - \frac{{\kappa_0}^2}{4} + \kappa\kappa_0\right)}$$

$$\beta_1 = i(\omega - \omega_{c1}) + \frac{|g_1|^2}{i(\omega - \omega_{r1}) - \gamma}$$

$$\beta_2 = i(\omega - \omega_{c2}) + \frac{|g_2|^2}{i(\omega - \omega_{r2}) - \gamma}$$

$$\begin{pmatrix} \hat{b}_{in}(\omega) \\ \hat{b}_{out}(\omega) \end{pmatrix} = \frac{1}{\beta_2 - \Gamma + \kappa_2} \begin{pmatrix} -\kappa_2 & \beta_2 - \Gamma \\ \beta_2 - \Gamma + 2\kappa_2 & \kappa_2 \end{pmatrix} \begin{pmatrix} 0 & e^{j2\pi} \\ e^{j2\pi} & 0 \end{pmatrix} \frac{1}{\beta_1 - \Gamma + \kappa_1} \begin{pmatrix} -\kappa_1 & \beta_1 - \Gamma \\ \beta_1 - \Gamma + 2\kappa_1 & \kappa_1 \end{pmatrix} \begin{pmatrix} \hat{a}_{in}(\omega) \\ \hat{a}_{out}(\omega) \end{pmatrix}$$

$$\begin{pmatrix} \hat{b}_{in}(\omega) \\ \hat{b}_{out}(\omega) \end{pmatrix} = \frac{1}{\beta_2 - \Gamma + \kappa_2} \frac{1}{\beta_1 - \Gamma + \kappa_1} \begin{pmatrix} \beta_2 - \Gamma & -\kappa_2 \\ -\kappa_2 & \beta_2 - \Gamma + 2\kappa_2 \end{pmatrix} \begin{pmatrix} -\kappa_1 & \beta_1 - \Gamma \\ \beta_1 - \Gamma + 2\kappa_1 & \kappa_1 \end{pmatrix} \begin{pmatrix} \hat{a}_{in}(\omega) \\ \hat{a}_{out}(\omega) \end{pmatrix}$$

$$m = \frac{1}{\beta_2 - \Gamma + \kappa_2} \frac{1}{\beta_1 - \Gamma + \kappa_1}$$

$$\begin{pmatrix} \hat{b}_{in}(\omega) \\ \hat{b}_{out}(\omega) \end{pmatrix} = m \begin{pmatrix} \beta_2 - \Gamma & -\kappa_2 \\ -\kappa_2 & \beta_2 - \Gamma + 2\kappa_2 \end{pmatrix} \begin{pmatrix} -\kappa_1 & \beta_1 - \Gamma \\ \beta_1 - \Gamma + 2\kappa_1 & \kappa_1 \end{pmatrix} \begin{pmatrix} \hat{a}_{in}(\omega) \\ \hat{a}_{out}(\omega) \end{pmatrix}$$

$$\begin{pmatrix} \hat{b}_{in}(\omega) \\ \hat{b}_{out}(\omega) \end{pmatrix} = m \begin{pmatrix} -\kappa_1(\beta_2 - \Gamma) - \kappa_2(\beta_1 - \Gamma + 2\kappa_1) & (\beta_1 - \Gamma)(\beta_2 - \Gamma) - \kappa_2\kappa_1 \\ -\kappa_2\kappa_1 + (\beta_2 - \Gamma + 2\kappa_2)(\beta_1 - \Gamma + 2\kappa_1) & \kappa_2(\beta_1 - \Gamma) + \kappa_1(\beta_2 - \Gamma + 2\kappa_2) \end{pmatrix} \begin{pmatrix} \hat{a}_{in}(\omega) \\ \hat{a}_{out}(\omega) \end{pmatrix}$$

$$\hat{b}_{in}(\omega) = m[\hat{a}_{in}(\omega)\,(-\kappa_1(\beta_2 - \Gamma) - \kappa_2(\beta_1 - \Gamma + 2\kappa_1)) + \hat{a}_{out}(\omega)(\beta_1 - \Gamma)(\beta_2 - \Gamma) - \kappa_2\kappa_1]$$

$$\hat{b}_{out}(\omega) = m\big[\hat{a}_{in}(\omega)\big(-\kappa_2\kappa_1 + (\beta_2 - \Gamma + 2\kappa_2)(\beta_1 - \Gamma + 2\kappa_1)\big) + \hat{a}_{out}(\omega)\,(\kappa_2(\beta_1 - \Gamma) + \kappa_1(\beta_2 - \Gamma + 2\kappa_2)\,)\big]$$

$$\hat{b}_{in}(\omega) = 0$$

$$\hat{a}_{out}(\omega) = \frac{(\kappa_1(\beta_2 - \Gamma) + \kappa_2(\beta_1 - \Gamma + 2\kappa_1)}{[(\beta_1 - \Gamma)(\beta_2 - \Gamma) - \kappa_2\kappa_1]}\hat{a}_{in}(\omega)$$

$$\hat{b}_{out}(\omega) = m.\hat{a}_{in}(\omega)\left[\left(-\kappa_2\kappa_1 + (\beta_2 - \Gamma + 2\kappa_2)(\beta_1 - \Gamma + 2\kappa_1)\right) + \frac{(\kappa_1(\beta_2 - \Gamma) + \kappa_2(\beta_1 - \Gamma + 2\kappa_1)}{[(\beta_1 - \Gamma)(\beta_2 - \Gamma) - \kappa_2\kappa_1]}(\kappa_2(\beta_1 - \Gamma) + \kappa_1(\beta_2 - \Gamma + 2\kappa_2)\ )\right]$$

$$\kappa_2 = \kappa_1 = \kappa$$

$$\frac{\hat{b}_{out}(\omega)}{\hat{a}_{in}(\omega)} = m\left[\left(-\kappa^2 + (\beta_2 - \Gamma + 2\kappa)(\beta_1 - \Gamma + 2\kappa)\right) + \frac{(\kappa(\beta_2 - \Gamma) + \kappa(\beta_1 - \Gamma + 2\kappa)}{[(\beta_1 - \Gamma)(\beta_2 - \Gamma) - \kappa^2]}\ (\kappa(\beta_1 - \Gamma) + \kappa(\beta_2 - \Gamma + 2\kappa_2)\ )\right]$$

$$\frac{\hat{b}_{out}(\omega)}{\hat{a}_{in}(\omega)} = m\left[a + \frac{b}{c}.d\right] = m\left[\frac{a.c + b.d}{c}\right]$$

$$a.c = -\kappa^2(\beta_1 - \Gamma)(\beta_2 - \Gamma) + \kappa^4 - \kappa^2(\beta_1 - \Gamma + 2\kappa)(\beta_2 - \Gamma + 2\kappa) + (\beta_2 - \Gamma + 2\kappa)(\beta_1 - \Gamma + 2\kappa)(\beta_1 - \Gamma)(\beta_2 - \Gamma)$$

$$b.d = \kappa^2(\beta_1 - \Gamma)(\beta_2 - \Gamma) + \kappa^2(\beta_2 - \Gamma)(\beta_2 - \Gamma + 2\kappa) + \kappa^2(\beta_1 - \Gamma)(\beta_1 - \Gamma + 2\kappa) + \kappa^2(\beta_2 - \Gamma + 2\kappa)\ (\beta_2 - \Gamma + 2\kappa)$$

$$a.c + b.d = \kappa^4 + (\beta_2 - \Gamma + 2\kappa)(\beta_1 - \Gamma + 2\kappa)(\beta_1 - \Gamma)(\beta_2 - \Gamma) + \kappa^2(\beta_2 - \Gamma)(\beta_2 - \Gamma + 2\kappa) + \kappa^2(\beta_1 - \Gamma)(\beta_1 - \Gamma + 2\kappa)$$

$$a.c + b.d = \kappa^2\ [\kappa^2 + (\beta_1 - \Gamma)(\beta_1 - \Gamma + 2\kappa)] + (\beta_2 - \Gamma)(\beta_2 - \Gamma + 2\kappa)[\kappa^2 + (\beta_1 - \Gamma)(\beta_1 - \Gamma + 2\kappa)]$$

$$a.c + b.d = [\kappa^2 + (\beta_2 - \Gamma)(\beta_2 - \Gamma + 2\kappa)].[(\kappa^2 + (\beta_1 - \Gamma)(\beta_1 - \Gamma + 2\kappa)]$$

$$a.c + b.d = [\kappa^2 + 2\kappa(\beta_2 - \Gamma) + (\beta_2 - \Gamma)^2].[\kappa^2 + 2\kappa(\beta_1 - \Gamma) + (\beta_1 - \Gamma)^2] = (\kappa + \beta_2 - \Gamma)^2.(\kappa + \beta_1 - \Gamma)^2$$

$$\frac{\hat{b}_{out}(\omega)}{\hat{a}_{in}(\omega)} = \frac{1}{\beta_2 - \Gamma + \kappa}\frac{1}{\beta_1 - \Gamma + \kappa}\frac{(\kappa + \beta_2 - \Gamma)^2.(\kappa + \beta_1 - \Gamma)^2}{[(\beta_1 - \Gamma)(\beta_2 - \Gamma) - \kappa^2]} = \frac{(\kappa + \beta_2 - \Gamma).(\kappa + \beta_1 - \Gamma)}{[(\beta_1 - \Gamma)(\beta_2 - \Gamma) - \kappa^2]}$$

$g_1 = 0$ and $\omega_{c2} = \omega_{r2} = \omega_{c1=0}$

If we rewrite the β_1 and β_2 equations for this given values.

$\beta_1 = i\omega$ and $\beta_2 = i\omega + \frac{|g|^2}{i\omega - \gamma}$

the general transmission equation is the same as classical EIT except the β values cause both of them have double cavities

$$\frac{\hat{b}_{out}}{\hat{a}_{in}} = \frac{(\kappa + \beta_1 - \Gamma)(\kappa + \beta_2 - \Gamma)}{(\beta_1 - \Gamma)(\beta_2 - \Gamma) - \kappa^2} = \frac{(\kappa + i\omega - \Gamma)\left(\kappa + i\omega + \frac{|g|^2}{i\omega - \gamma} - \Gamma\right)}{(i\omega - \Gamma)\left(i\omega + \frac{|g|^2}{i\omega - \gamma} - \Gamma\right) - \kappa^2}$$

$$= \frac{(\kappa + i\omega - \Gamma)(\kappa i\omega - \kappa\gamma - \omega^2 + i\omega\gamma + g^2 - \Gamma i\omega + \gamma\Gamma)}{\left[\left((i\omega - \Gamma)\right)(-\omega^2 + i\omega\gamma + g^2 - \Gamma i\omega + \gamma\Gamma)\right] - \kappa^2}$$

$$a.c + b.d = [\kappa^2 + (\beta_2 - \Gamma)(\beta_2 - \Gamma + 2\kappa)].[(\kappa^2 + (\beta_1 - \Gamma)(\beta_1 - \Gamma + 2\kappa)]$$

$$\frac{\hat{b}_{out}}{\hat{a}_{in}} = \frac{a+bi}{c+di} = \frac{1}{c^2+d^2}(ac+db+i(bc-da)) = x+yi$$

if trans$= x+yi$

$$\theta = \tan^{-1}(y/x)$$

$$\frac{d}{d\omega}(\theta) = \frac{d}{d\omega}\left(\tan^{-1}(y/x)\right) = \frac{\left(y/x\right)'}{1+\left(y/x\right)^2} = \frac{y'x-x'y}{y^2+x^2}$$

$$y= \omega\left(-\omega^2+g^2+\frac{5\kappa_0{}^2}{4}\right)\left(2\omega^2\kappa_0-2\kappa\omega^2-\kappa g^2-\frac{g^2\kappa_0}{2}-\kappa\kappa_0{}^2-\frac{\kappa_0{}^3}{4}\right)-\left(2\omega^2\kappa_0-\frac{g^2\kappa_0}{2}-\frac{\kappa_0{}^3}{4}\right)\omega\left(g^2-\omega^2+3\kappa\kappa_0-\frac{5\kappa_0{}^2}{4}\right)$$

$$x=\left(2\omega^2\kappa_0-\frac{g^2\kappa_0}{2}-\frac{\kappa_0{}^3}{4}\right)\left(2\omega^2\kappa_0-2\kappa\omega^2-\kappa g^2-\frac{g^2\kappa_0}{2}-\kappa\kappa_0{}^2-\frac{\kappa_0{}^3}{4}\right)+\omega\left(-\omega^2+g^2+\frac{5\kappa_0{}^2}{4}\right)\omega\left(g^2-\omega^2+3\kappa\kappa_0-\frac{5\kappa_0{}^2}{4}\right)$$

$$\begin{pmatrix}\hat{b}_{in}(\omega)\\ \hat{b}_{out}(\omega)\end{pmatrix} = \frac{1}{\beta_3-\Gamma+\kappa_3}\begin{pmatrix}-\kappa_3 & \beta_3-\Gamma\\ \beta_3-\Gamma+2\kappa_3 & \kappa_3\end{pmatrix}\begin{pmatrix}0 & e^{j2\pi}\\ e^{j2\pi} & 0\end{pmatrix}$$

$$\frac{1}{\beta_2-\Gamma+\kappa_2}\begin{pmatrix}-\kappa_2 & \beta_2-\Gamma\\ \beta_2-\Gamma+2\kappa_2 & \kappa_2\end{pmatrix}\begin{pmatrix}0 & e^{j2\pi}\\ e^{j2\pi} & 0\end{pmatrix}$$

$$\frac{1}{\beta_1-\Gamma+\kappa_1}\begin{pmatrix}-\kappa_1 & \beta_1-\Gamma\\ \beta_1-\Gamma+2\kappa_1 & \kappa_1\end{pmatrix}\begin{pmatrix}\hat{a}_{in}(\omega)\\ \hat{a}_{out}(\omega)\end{pmatrix}$$

$$m = \frac{1}{(\beta_1-\Gamma+\kappa_1)}\frac{1}{(\beta_3-\Gamma+\kappa_2)}\frac{1}{(\beta_3-\Gamma+\kappa_3)}$$

$$\begin{pmatrix}\hat{b}_{in}(\omega)\\ \hat{b}_{out}(\omega)\end{pmatrix} = m\begin{pmatrix}\beta_3-\Gamma & -\kappa_3\\ \kappa_3 & \beta_3-\Gamma+2\kappa_3\end{pmatrix}\begin{pmatrix}\beta_2-\Gamma & -\kappa_2\\ \kappa_2 & \beta_2-\Gamma+2\kappa_2\end{pmatrix}\begin{pmatrix}-\kappa_1 & \beta_1-\Gamma\\ \beta_1-\Gamma+2\kappa_1 & -\kappa_1\end{pmatrix}\begin{pmatrix}\hat{a}_{in}(\omega)\\ \hat{a}_{out}(\omega)\end{pmatrix}$$

$$\kappa_3 = \kappa_2 = \kappa_1 = \kappa$$

$$\begin{pmatrix}\hat{b}_{in}(\omega)\\ \hat{b}_{out}(\omega)\end{pmatrix} = m*h$$

$$h=\begin{pmatrix}(\beta_3-\Gamma)(\beta_2-\Gamma)-\kappa^2 & -\kappa(\beta_3-\Gamma)-\kappa(\beta_2-\Gamma+2\kappa)\\ -\kappa(\beta_2-\Gamma)+\kappa(\beta_3-\Gamma+2\kappa) & -\kappa^2+(\beta_3-\Gamma+2\kappa_3)(\beta_2-\Gamma+2\kappa)\end{pmatrix}\begin{pmatrix}-\kappa & \beta_1-\Gamma\\ \beta_1-\Gamma+2\kappa & \kappa\end{pmatrix}\begin{pmatrix}\hat{a}_{in}(\omega)\\ \hat{a}_{out}(\omega)\end{pmatrix}$$

$$\begin{pmatrix}\hat{b}_{in}(\omega)\\ \hat{b}_{out}(\omega)\end{pmatrix} = m\begin{pmatrix}a & b\\ c & d\end{pmatrix}\begin{pmatrix}\hat{a}_{in}(\omega)\\ \hat{a}_{out}(\omega)\end{pmatrix}$$

$$a = -\kappa[(\beta_3 - \Gamma)(\beta_2 - \Gamma) - \kappa^2] - \kappa[(\beta_3 - \Gamma) + (\beta_2 - \Gamma + 2\kappa)](\beta_1 - \Gamma + 2\kappa)$$

$$b = [(\beta_3 - \Gamma)(\beta_2 - \Gamma) - \kappa^2](\beta_1 - \Gamma) - \kappa[(\beta_3 - \Gamma) + (\beta_2 - \Gamma + 2\kappa)]\,\kappa$$

$$c = [\kappa(\beta_2 - \Gamma) + (\beta_3 - \Gamma + 2\kappa)](-\kappa) + [-\kappa^2 + (\beta_3 - \Gamma + 2\kappa_3)(\beta_2 - \Gamma + 2\kappa)](\beta_1 - \Gamma + 2\kappa)$$

$$d = [\kappa(\beta_2 - \Gamma) + (\beta_3 - \Gamma + 2\kappa)](\beta_1 - \Gamma) + [-\kappa^2 + (\beta_3 - \Gamma + 2\kappa_3)(\beta_2 - \Gamma + 2\kappa)]\,\kappa$$

$$\hat{b}_{in}(\omega) = 0$$

$$\hat{a}_{out}(\omega) = -\frac{a}{b}\hat{a}_{in}(\omega) \qquad \hat{b}_{out}(\omega) = m.(c - \frac{a}{b}d)\hat{a}_{in}(\omega)$$

$$\frac{\hat{b}_{out}(\omega)}{\hat{a}_{in}(\omega)} = m.(\frac{b.c - d.a}{b})$$

$$b.c = -\kappa^2(\beta_3 - \Gamma)(\beta_2 - \Gamma)^2(\beta_1 - \Gamma) + \kappa^4(\beta_2 - \Gamma)(\beta_1 - \Gamma) + \kappa^4(\beta_3 - \Gamma)(\beta_2 - \Gamma) + \kappa^4(\beta_2 - \Gamma)(\beta_2 - \Gamma + 2\kappa)$$

$$-\kappa^2(\beta_3 - \Gamma)(\beta_2 - \Gamma)(\beta_1 - \Gamma)(\beta_3 - \Gamma + 2\kappa) + \kappa^4(\beta_1 - \Gamma)(\beta_3 - \Gamma + 2\kappa) + \kappa^4(\beta_3 - \Gamma)(\beta_3 - \Gamma + 2\kappa)$$

$$+\kappa^4(\beta_3 - \Gamma + 2\kappa) - \kappa^2(\beta_3 - \Gamma)(\beta_2 - \Gamma)(\beta_1 - \Gamma)(\beta_1 - \Gamma + 2\kappa) + \kappa^4(\beta_1 - \Gamma)(\beta_1 - \Gamma + 2\kappa)$$

$$+\kappa^4(\beta_3 - \Gamma)(1_3 - \Gamma + 2\kappa) + \kappa^4(\beta_3 - \Gamma + 2\kappa)(\beta_1 - \Gamma + 2\kappa)$$

$$+(\beta_3 - \Gamma)(\beta_2 - \Gamma)(\beta_1 - \Gamma)(\beta_3 - \Gamma + 2\kappa)(\beta_2 - \Gamma + 2\kappa)(\beta_1 - \Gamma + 2\kappa)$$

$$-\kappa^2(\beta_1 - \Gamma)(\beta_3 - \Gamma + 2\kappa)(\beta_2 - \Gamma + 2\kappa)(\beta_1 - \Gamma + 2\kappa)$$

$$-a.d=-\kappa^4(\beta_2-\Gamma)(\beta_1-\Gamma)+\kappa^4(\beta_3-\Gamma)(\beta_2-\Gamma)(\beta_1-\Gamma)(\beta_1-\Gamma+2\kappa)$$

$$+\kappa^2(\beta_2-\Gamma)(\beta_1-\Gamma)\left(\begin{matrix}\beta_2-\Gamma+\\ 2\kappa\end{matrix}\right)(\beta_1-\Gamma+2\kappa)+\kappa^2(\beta_3-\Gamma)(\beta_2-\Gamma)^2(\beta_1-\Gamma)$$

$$+\kappa^2(\beta_3-\Gamma)(\beta_2-\Gamma)(\beta_1-\Gamma)(\beta_3-\Gamma+2\kappa)-\kappa^4(\beta_1-\Gamma)(\beta_3-\Gamma+2\kappa)$$

$$+\kappa^2(\beta_3-\Gamma)(\beta_1-\Gamma)(\beta_3-\Gamma+2\kappa)(\beta_1-\Gamma+2\kappa)$$

$$+\kappa^2(\beta_1-\Gamma)(\beta_3-\Gamma+2\kappa)(\beta_2-\Gamma+2\kappa)(\beta_1-\Gamma+2\kappa)$$

$$+\kappa^4(\beta_3-\Gamma)(\beta_2-\Gamma)+\kappa^6-\kappa^4(\beta_3-\Gamma)(\beta_1-\Gamma+2\kappa)+\kappa^4(\beta_2-\Gamma+2\kappa)(\beta_1-\Gamma+2\kappa)$$

$$+\kappa^2(\beta_3-\Gamma)(\beta_2-\Gamma)(\beta_1-\Gamma)(\beta_3-\Gamma+2\kappa)-\kappa^4(\beta_1-\Gamma)(\beta_3-\Gamma+2\kappa)$$

$$+\kappa^2(\beta_3-\Gamma)(\beta_1-\Gamma)(\beta_3-\Gamma+2\kappa)(\beta_1-\Gamma+2\kappa)$$

$$+\kappa^2(\beta_1-\Gamma)(\beta_3-\Gamma+2\kappa)(\beta_2-\Gamma+2\kappa)(\beta_1-\Gamma+2\kappa)$$

$$b.c-a.d=\kappa^4(\beta_2-\Gamma)(\beta_2-\Gamma+2\kappa)+\kappa^4(\beta_3-\Gamma)(\beta_3-\Gamma+2\kappa)+\kappa^4(\beta_1-\Gamma)(\beta_1-\Gamma+2\kappa)$$

$$+(\beta_3-\Gamma)(\beta_2-\Gamma)(\beta_1-\Gamma)(\beta_3-\Gamma+2\kappa)(\beta_2-\Gamma+2\kappa)(\beta_1-\Gamma+2\kappa)$$

$$+\kappa^2(\beta_2-\Gamma)(\beta_1-\Gamma)(\beta_2-\Gamma+2\kappa)(\beta_1-\Gamma+2\kappa)$$

$$+\kappa^2(\beta_3-\Gamma)(\beta_1-\Gamma)(\beta_3-\Gamma+2\kappa)(\beta_1-\Gamma+2\kappa)+\kappa^6+\ \kappa^2(\beta_3-\Gamma)(\beta_2-\Gamma)(\beta_1-\Gamma)(\beta_3-\Gamma+2\kappa)$$

b.c-a.d=$\kappa^6 + \kappa^4 x + \kappa^4 y + \kappa^4 z + xyz + \kappa^2 xy + \kappa^2 yz + + \kappa^2 xz = (\kappa^2 + x)(\kappa^2 + y)(\kappa^2 + z)$

b.c-a.d= $(\kappa^2 + (\beta_1 - \Gamma)(\beta_1 - \Gamma + 2\kappa)).\left(\kappa^2 + (\beta_2 - \Gamma)(\beta_2 - \Gamma + 2\kappa)\right).(\kappa^2 + (\beta_3 - \Gamma)(\beta_3 - \Gamma + 2\kappa))$

b.c-a.d=$(\kappa + (\beta_1 - \Gamma))^2.(\kappa + (\beta_2 - \Gamma))^2.(\kappa + (\beta_3 - \Gamma))^2$

$$\frac{\hat{b}_{out}(\omega)}{\hat{a}_{in}(\omega)} = \frac{1}{(\beta_1 - \Gamma + \kappa_1)}\frac{1}{(\beta_3 - \Gamma + \kappa_2)}\frac{1}{(\beta_3 - \Gamma + \kappa_3)}.\frac{(\kappa + (\beta_1 - \Gamma))^2.(\kappa + (\beta_2 - \Gamma))^2.(\kappa + (\beta_3 - \Gamma))^2}{[(\beta_3 - \Gamma)(\beta_2 - \Gamma) - \kappa^2](\beta_1 - \Gamma) - \kappa[(\beta_3 - \Gamma) + (\beta_2 - \Gamma + 2\kappa)]\,\kappa}$$

$$\frac{\hat{b}_{out}(\omega)}{\hat{a}_{in}(\omega)} = \frac{(\kappa + (\beta_1 - \Gamma))(\kappa + (\beta_1 - \Gamma))(\kappa + (\beta_1 - \Gamma))}{(\beta_3 - \Gamma)(\beta_2 - \Gamma)(\beta_1 - \Gamma) - \kappa^2(\beta_1 - \Gamma) - \kappa^2(\beta_3 - \Gamma) + \kappa^2\,(\beta_2 - \Gamma) - 2\kappa^3}$$

$g_1 = g_2 = g_3 = 0, \beta_1 = i(\omega + \Delta\omega), \beta_2 = 0$

$\beta_3 = i(\omega - \Delta\omega)$

$$\frac{\hat{b}_{out}(\omega)}{\hat{a}_{in}(\omega)} = \frac{(\kappa + (\beta_1 - \Gamma))(\kappa + (\beta_1 - \Gamma))(\kappa + (\beta_1 - \Gamma))}{(\beta_3 - \Gamma)(\beta_2 - \Gamma)(\beta_1 - \Gamma) - \kappa^2(\beta_1 - \Gamma) - \kappa^2(\beta_3 - \Gamma) + \kappa^2\,(\beta_2 - \Gamma) - 2\kappa^3}$$

$$\frac{\hat{b}_{out}(\omega)}{\hat{a}_{in}(\omega)} = \frac{(\kappa + (\beta_1 - \Gamma))(\kappa + (\beta_1 - \Gamma))(\kappa + (\beta_1 - \Gamma))}{(\beta_3 - \Gamma)(\beta_2 - \Gamma)(\beta_1 - \Gamma) - \kappa^2(\beta_1+\beta_2+\beta_3 - 3\Gamma) - 2\kappa^3}$$

$$\frac{\hat{b}_{out}(\omega)}{\hat{a}_{in}(\omega)} = \frac{(\kappa + i(\omega + \Delta\omega) - \Gamma)(\kappa + i(\omega - \Delta\omega) - \Gamma)(\kappa + i\omega - \Gamma)}{(i(\omega + \Delta\omega) - \Gamma)(i(\omega - \Delta\omega) - \Gamma)(i\omega - \Gamma) - \kappa^2(i(\omega + \Delta\omega) + i(\omega - \Delta\omega) + i\omega - 3\Gamma) - 2\kappa^3}$$

$$\frac{\hat{b}_{out}(\omega)}{\hat{a}_{in}(\omega)} = \frac{\kappa^3 - 3\kappa^2\Gamma + 3\Gamma^2\kappa - 3\omega^2\kappa + 3\omega^2\Gamma - \Gamma^3 - \Delta\omega^2\Gamma + \Delta\omega^2\kappa}{(i(\omega+\Delta\omega)-\Gamma)(i(\omega-\Delta\omega)-\Gamma)(i\omega-\Gamma) - \kappa^2(i(\omega+\Delta\omega)+i(\omega-\Delta\omega)+i\omega-3\Gamma) - 2\kappa^3}$$

$$\text{trans}(\omega) = \frac{\left(\frac{3}{2}\omega^2\kappa_0 - \frac{1}{8}{\kappa_0}^3 - \frac{1}{2}\kappa_0\Delta\omega^2\right) + i\omega\left(-\omega^2 + \frac{3}{4}{\kappa_0}^2 + \Delta\omega^2\right)}{\left(3\omega^2\kappa + \frac{3}{2}\omega^2\kappa_0 - \frac{3}{4}\kappa{\kappa_0}^2 - \frac{1}{8}{\kappa_0}^3 - \Delta\omega^2\kappa - \frac{1}{2}\kappa_0\Delta\omega^2\right) - i\omega\left(\omega^2 - 3\kappa\kappa_0 - \frac{3}{4}{\kappa_0}^2 - \Delta\omega^2\right)}$$

$$\frac{\tau_c}{\tau_{life}} = \left(\frac{y'x - x'y}{x^2 + y^2}\right) * (2\kappa + \kappa_0)$$

$$x = \left(\frac{3}{2}\omega^2\kappa_0 - \frac{1}{8}{\kappa_0}^3 - \frac{1}{2}\kappa_0\Delta\omega^2\right)\left(3\omega^2\kappa + \frac{3}{2}\omega^2\kappa_0 - \frac{3}{4}\kappa{\kappa_0}^2 - \frac{1}{8}{\kappa_0}^3 - \Delta\omega^2\kappa - \frac{1}{2}\kappa_0\Delta\omega^2\right)$$

$$+\omega\left(-\omega^2 + \frac{3}{4}{\kappa_0}^2 + \Delta\omega^2\right)\omega\left(g^2 - \omega^2 + 3\kappa\kappa_0 - \frac{5}{4}{\kappa_0}^2\right)$$

$$x' = (3\omega\kappa_0)\left(3\omega^2\kappa + \frac{3}{2}\omega^2\kappa_0 - \frac{3}{4}\kappa{\kappa_0}^2 - \frac{1}{8}{\kappa_0}^3 - \Delta\omega^2\kappa - \frac{1}{2}\kappa_0\Delta\omega^2\right) + \left(\frac{3}{2}\omega^2\kappa_0 - \frac{1}{8}{\kappa_0}^3 - \frac{1}{2}\kappa_0\Delta\omega^2\right)(6\omega\kappa + 3\omega\kappa_0)$$

$$+(-3\omega^2)\omega\left(g^2 - \omega^2 + 3\kappa\kappa_0 - \frac{5}{4}{\kappa_0}^2\right) + \omega\left(-\omega^2 + \frac{3}{4}{\kappa_0}^2 + \Delta\omega^2\right)(-3\omega^2)$$

$$y = \omega\left(-\omega^2 + \frac{3}{4}{\kappa_0}^2 + \Delta\omega^2\right)\left(3\omega^2\kappa + \frac{3}{2}\omega^2\kappa_0 - \frac{3}{4}\kappa{\kappa_0}^2 - \frac{1}{8}{\kappa_0}^3 - \Delta\omega^2\kappa - \frac{1}{2}\kappa_0\Delta\omega^2\right)$$

$$-\left(\frac{3}{2}\omega^2\kappa_0 - \frac{1}{8}{\kappa_0}^3 - \frac{1}{2}\kappa_0\Delta\omega^2\right)\left(g^2 - \omega^2 + 3\kappa\kappa_0 - \frac{5}{4}{\kappa_0}^2\right)$$

$$y' = (-3\omega^2)\left(3\omega^2\kappa + \frac{3}{2}\omega^2\kappa_0 - \frac{3}{4}\kappa{\kappa_0}^2 - \frac{1}{8}{\kappa_0}^3 - \Delta\omega^2\kappa - \frac{1}{2}\kappa_0\Delta\omega^2\right) + \omega\left(-\omega^2 + \frac{3}{4}{\kappa_0}^2 + \Delta\omega^2\right)(6\omega\kappa + 3\omega\kappa_0)$$

$$-[(3\omega\kappa_0)\left(g^2 - \omega^2 + 3\kappa\kappa_0 - \tfrac{5}{4}{\kappa_0}^2\right) + \left(\tfrac{3}{2}\omega^2\kappa_0 - \tfrac{1}{8}{\kappa_0}^3 - \tfrac{1}{2}\kappa_0\Delta\omega^2\right)(-3\omega^2)]$$

$$t(\omega) = \frac{\left(2\omega^2\kappa_0 - \frac{1}{2}g^2\kappa_0\right) + i\omega(-\omega^2 + g^2)}{(2\kappa\omega^2 - \kappa g^2) + i\omega(g^2 - \omega^2)}$$

$$t(\omega) = \frac{\left(\frac{3}{2}\omega^2\kappa_0 - \frac{1}{2}\kappa_0\Delta\omega^2\right) + i\omega(-\omega^2 + \Delta\omega^2)}{(3\omega^2\kappa - \Delta\omega^2\kappa) + i\omega(\Delta\omega^2 - \omega^2)}$$